Role of PET/CT in Pediatric Malignancy

21

Joe Barfett, Reza Vali, and Amer Shammas

Contents

21.1 **Introduction** 538

21.2 **Functional Versus Anatomic Imaging in Pediatric Malignancy** 538

21.3 **Special Considerations in the Pediatric Population** 540
21.3.1 Radiation Dose 540
21.3.2 Sedation 541
21.3.3 Special Considerations in ^{18}F-FDG PET/CT 541
21.3.4 Isotopes and Radiopharmaceuticals 542
21.3.5 Protocols for Fluorodeoxyglucose PET ... 542
21.3.6 F18-FDG PET Normal Variants and Pitfalls in Children 543
21.3.7 Standardized Uptake Values 543
21.3.8 Thymus 544
21.3.9 Tonsils 545
21.3.10 Marrow Hyperplasia 545
21.3.11 Brown Fat 545
21.3.12 Posttreatment Change 546
21.3.13 Other Pitfalls 546
21.3.14 Other Radiopharmaceuticals 547

21.4 **Image Fusion** 549

21.5 **Tumors of the Sympathetic Nervous System** 549
21.5.1 Neuroblastoma 549
21.5.2 Pheochromocytoma 553

21.6 **Lymphoma** 554
21.6.1 Hodgkin's Disease 554
21.6.2 Non-Hodgkin's Lymphoma 555
21.6.3 Initial Staging with ^{18}F-FDG PET/CT 556
21.6.4 Evaluation of Therapy Response with ^{18}F-FDG PET/CT 557
21.6.5 Evaluation of Relapse or Recurrence 558
21.6.6 Posttransplant Lymphoproliferative Disorder 558

21.7 **Leukemia** 560

21.8 **Tumors of the Brain and Central Nervous System** 560

21.9 **Osseous and Soft Tissue Malignancy** 562
21.9.1 Osteosarcoma 563
21.9.2 Ewing's Sarcoma 564
21.9.3 Rhabdomyosarcoma 565

21.10 **Nephroblastoma (Wilms' Tumor)** 566

21.11 **Hepatoblastoma** 566

21.12 **Thyroid Malignancy** 567

Conclusion 567

References 568

J. Barfett
Saint Michael Hospital, University of Toronto, Toronto, ON, Canada

R. Vali • A. Shammas (✉)
The Hospital for Sick Children, University of Toronto, Toronto, ON, Canada
e-mail: reza.vali@sickkids.ca; amer.shammas@sickkids.ca

Abstract

Positron emission tomography (PET)/computed tomography (CT) is emerging as an important noninvasive imaging modality for assessing a wide variety of malignancies in both adults and children. However, a different approach may be needed in children than that

M.M. Khalil (ed.), *Basic Science of PET Imaging*, DOI 10.1007/978-3-319-40070-9_21

of adults due to vulnerability of children to radiation, different types of malignancies in pediatric population comparing with adults, and special technical issues and pitfalls in pediatric PET/CT imaging. In this chapter, we discuss special considerations in pediatric PET/CT imaging and explore the use of FDG-PET in pediatric malignancies, including lymphomas, sympathetic nervous system tumors, bone and soft tissue sarcomas, neuroblastomas, and the less-common tumors, such as thyroid cancers, Wilms' tumors, and hepatoblastomas.

21.1 Introduction

Although the incidence of childhood malignancy is quite low, approximately 130 per million children in the United States [1], cancer remains the second most common cause of death in children age 1–14 years [2], second only to accidental death. The International Classification of Childhood Cancer (ICCC) categorizes pediatric malignancy into 12 major groups [3] including leukemias, brain and central nervous system malignancy, lymphomas, soft tissue sarcoma, tumors of the sympathetic nervous system, renal tumors, bone tumors, carcinoma and melanoma, germ cell tumors, retinoblastoma, hepatic tumors, and other or unspecified tumors (Table 21.1). Leukemia, central nervous system cancer, and lymphoma are the three most common forms of childhood cancer, accounting for 30, 20, and 14 % of overall incidence [4]. Outcome in these three particular malignancies has improved markedly in past decades and has contributed to an overall increase in 5-year survival from 58 % in 1977 to 83 % in 2007 [5].

The overall incidence of pediatric malignancy is increasing and has escalated from 0.5 % to approximately 1 % over the past 30 years with most of this increase having occurred in carcinoma, lymphoma, and germ cell tumors [4]. The reasons for this increase are not understood, and the pessimistic natural history of most pediatric cancers weighs against improvements in tracking and documentation of statistics as the sole cause.

Nuclear medicine and specifically positron emission tomography (PET) imaging have played a major role in the improved detection and staging of malignancy [6]. Thus PET/CT imaging is of pivotal importance in all pediatric cancer centers for most malignancies. A wealth of new PET tracers is on the horizon which promises to significantly expand the molecular imaging toolbox [7–9]. (See Chap. 17 for more details about new emerging PET tracers.)

21.2 Functional Versus Anatomic Imaging in Pediatric Malignancy

Although ultrasound is widely used in the initial detection of pediatric malignancy, CT and MR imaging remain the standard of care for the initial staging of most tumors, with the possible exception of leukemia as discussed below. As opposed to "emission tomography" which is common in nuclear medicine, computed tomography is a form of "transmission tomography" relying upon X-rays with energies generally between 60 and 140 keV depending primarily on the body habitus of the patient. As an X-ray imaging modality, CT images the spatial distribution of density, which is often significantly altered by malignancy. In addition, iodinated contrast enables the assessment of both the vascularity and, generally in a nonquantitative fashion, capillary permeability of structures under examination. 4D CT, which can potentially rigorously calculate perfusion and capillary leak in malignancy [10], is seldom used in the pediatric population due to the implicit relatively high radiation exposure and the short time over which that dose is applied. Where iodinated contrast is employed, the tube energy is often set to approximate the 32 keV K-edge of iodine [11] to maximize visibility of the agent as closely as possible while maintaining acceptable image quality. Dual energy CT, an old technique with fairly recent implementation in clinical practice, enables multi-element decomposition and can

Table 21.1 Age-adjusted and age-specific SEER Cancer Incidence Rates, 2005–2009 by the International Classification of Childhood Cancer (ICCC) http://seer.cancer.gov/csr/1975_2009_pops09/results_merged/sect_29_childhood_cancer_iccc.pdf

No.	Type of malignancy	Percentage (%)	0–14[a]	0–19[a]	5-year survival[b]
1	Leukemias	30	51.6	47.1	80.7
2	Brain and CNS tumors	20	42.2	43.1	72.1
3	lymphomas	14	16.6	25.1	90.0
4	Soft tissue sarcomas	7	10.9	12.4	71.0
5	SNS tumors	7	10.2	7.8	75.4
6	Renal tumors	6	7.8	6.3	88.8
7	Osseous tumors	5	7.3	9.2	69.0
8	Carcinomas	3	6.7	17.1	92.7
9	Germ cell tumors	3	5.7	11.9	91.2
10	Retinoblastomas	3	4.1	3.1	97.8
11	Hepatic tumors	1	2.5	2.2	68.2
12	Others	1	0.5	0.5	

[a]Rates are per 1,000,000 and are age adjusted to the 2000 US Std Population (19 age groups – Census P25-1130)
[b]5-Year Relative Survival (Percent), 2002–2008 by International Classification of Childhood Cancer(ICCC) Selected Group and Subgroup and Sex and Age. Benign brain and myelodysplastic syndromes are excluded

potentially supplement structural imaging with "iodine maps" which may offer improved routine assessment of these functional parameters at routine dose [12]. In CT, because the acquisition is so fast, problems such as patient motion or a mistimed contrast bolus which are common in pediatric imaging can only be corrected by repeat scanning which entails a second radiation dose. Low-dose CT is however extensively used in nuclear imaging for anatomic localization and attenuation correction and being an attenuation-based modality carries a technical advantage over MRI in this regard [13].

Conventional MR images the spatial distribution of hydrogen in water molecules using a hydrogen coil and strong magnetic fields. Unlike CT images, which can be acquired in seconds, a complete MRI requires several minutes to sometimes over an hour to acquire depending on the size of the imaging field, number and type of sequences chosen, and whether gadolinium-enhanced images are required. Thus sedation is often necessary in children, in our experience, under the age of 6 even with a skilled technologist. Although exquisite contrast resolution is available in MRI (unlike CT which offers better spatial resolution), MRI does not image tissue density directly and so carries limitations in terms of attenuation correction of nuclear images including PET. These limitations can potentially be overcome with appropriate software [14]. MRI is capable of high-end functional imaging including perfusion imaging, the imaging of molecular motion, intravascular flow assessment, and blood-oxygen-level-dependent (BOLD) imaging and offers numerous extensively described though more experimental techniques such as arterial spin labeling to assess perfusion without contrast, as well as thermometry to assess metabolic activity in the form of heat. It is important to note however that from a clinical point of view, none of these advanced tools has been shown to outperform PET/CT imaging clinically for the staging of disease or assessment of treatment response. Despite the power of MRI particularly in the brain, PET has remained a useful tool in addition to MRI to assess brain tumors for histologic grade, response to therapy, and recurrence [15–17]. In addition, because MRI is affected by signal dropout next to air, metal, or dense calcium, MRI is limited to assess the lung parenchyma, mucosal interfaces, or bone/tissue adjacent to orthopedic hardware [18–20].

Conversely nuclear imaging, especially PET when coupled with CT, excels in these technically challenging situations. In addition, PET

images which are limited by problems such as motion artifact can often simply be reacquired without additional dose to the patient. All imaging modalities including CT, MRI, conventional nuclear imaging, and PET should be regarded as complimentary tools in a well-equipped imaging department, each with their own strengths.

21.3 Special Considerations in the Pediatric Population

Obtaining high-quality studies in children is both challenging and rewarding. It is important to understand that in pediatric nuclear medicine, the staff is working with both frightened child and anxious parents. Careful planning (including a flexible scheduling), communication appropriate for the child's stage of development, appropriate injection techniques, paying attention to the imaging environment (including the use of immobilization devices or safety restraints, distraction techniques, and the possibility of sedation when necessary), and a friendly atmosphere are the key factors to deal with children and their parents. In general, it takes about twice as long to complete a procedure on a pediatric patient as on an adult.

21.3.1 Radiation Dose

Although the oncogenic potential of ionizing radiation is a function of age, with younger patients being at higher risk than older patients, the likelihood of secondary malignancy arising as a result of diagnostic medical radiation exposure, even in children, is so low as to be statistically difficult to calculate [21]. Studies published to date claiming an association between medical radiation and cancer are influenced by controversial statistical assumptions or selection bias [6].

Studies assuming a linear no-threshold model of radiation injury deemed to be a conservative view by the International Commission on Radiological Protection and back-projecting atomic bomb and nuclear accident cancer risks are deemed by some authors as inappropriate [6]. These studies are contradicted by many years of high-dose I131 therapy data for hyperthyroidism which has failed to demonstrate any definite increase in cancer risk [22, 23].

Two principles can however be universally agreed upon:

1. Test only when truly medically indicated.
2. When testing, use as low a radiation dose as is reasonably achievable (ALARA).

ALARA applies to technologists and physicians as much as it applies to patients [24].

Although children are more radiosensitive than adults [25], nuclear medicine tracers have an advantage over X-ray imaging techniques such as CT in that the dose is applied over a longer duration [26]. Double-stranded DNA breaks, which are repaired over 1–4 h at diagnostic doses, may not compound with each other as readily in any given cell if a patient is radiated over hours (i.e., ^{18}F-FDG PET), days (i.e., Tc 99m), or weeks (i.e., Ga 67) for any given cumulative dose in mSv [27].

Shorter half-lives result in decreased cumulative dose. It is preferable for diagnostic purposes to avoid isotopes which emit beta or alpha particles, and as such I123 is strongly favored over I131 for scintigraphic applications. PET imaging in general employs shorter half-life tracers than conventional nuclear medicine imaging and benefits, on the whole, from a corresponding dose reduction, particularly where many of the on-site cyclotrons produced short half-life isotopes are concerned. PET dosimetry is discussed in Chap. 3.

An important caveat to the above however is in special populations, for example, children with known mutations inhibiting proper DNA repair. A classic example is retinoblastoma, where patients are so radiosensitive as to avoid sun and X-ray exposure as well as other sources of oxidative injury [28, 29]. In adults, the classic example is BRCA mutation, which is likely associated with increased radiosensitivity [30, 31]. Such special populations do become a major issue in specialized tertiary and quaternary pediatric hospitals. In these patients, there may be particularly

aggressive application of ALARA, and MRI with sedation may in some instances be preferable to ionizing radiation exposure.

In 2015, it is no longer reasonable to assume that iodinated contrast media and gadolinium-based contrast agents do not produce oxidative DNA injury [32]. These agents produce the same double-stranded DNA injury as does radiation exposure, alcohol consumption [33], toxin exposure including smoking, and excessive exercise [34], all of which are discouraged in children and young adults.

The pediatric injected dose are usually calculated from the adult dose based on different formulas adjusting for weight ((body mass (kg) × adult dose)/70 kg), body surface area ((BSA (m^2) × adult dose)/1.73 m^2), age (Webster's formula; (age (years) + 7) × (adult dose)/(age (years) + 1)), or the European Association of Nuclear Medicine (EANM) Paediatric Dose Card [35–37]. With the new technology and improved instrumentation, the optimum doses for children should be changed. This was addressed in the new North American consensus guidelines published in 2010 [38]. However, the selection of the appropriate dose depends on the patient population, choice of equipment, specific requirements of the clinical protocols, and the physician's judgment [35]. Thus, deviation from the administered activities listed in the consensus guidelines can be considered appropriate when clinically indicated [35].

21.3.2 Sedation

Pharmacologic sedation can be kept to a minimum with adequate patient preparation, patient and parent education, as well as technologists that are experienced in the care of children. When absolutely necessary, the most commonly used drugs include midazolam, oral chloral hydrate, and pentobarbital [39, 40]. Patients > 15 kg with developmental delay are also most commonly sedated with either midazolam or pentobarbital [39, 40]. Pentobarbital, as all barbiturates, is contraindicated in patients with porphyria. Seizure patients subjected to pentobarbital may require dose adjustments or tapering of dose [40].

In addition to its sedative and anxiolytic effects, benzodiazepines such as midazolam have useful amnestic effect which can be particularly helpful if a patient must be exposed to multiple repeat tests in an imaging department [40]. In general each center will have its own guidelines on the sedation of children. For reference, the American Academy of Pediatrics (AAP) also publishes useful guidelines which guide best practices. Institutional protocols should be developed in collaboration with anesthesiology and include the availability of reversal drugs [39]. The continuing support and availability of anesthesiology is of immense benefit to a nuclear medicine department specializing in the care of children.

Patients with risk factors for anesthesia, including but not limited to airway obstruction, snoring, cardiorespiratory illness of any kind, asthma, intracranial pressure abnormality, or altered neck biomechanics, would benefit the most from real-time monitoring by a qualified anesthetist. Risks such as malignant hyperthermia should also be considered [40]. Playing with the patient; providing a pacifier, bottle, or (preferably non attenuating) toy; the use of distractors including nap time and room decorations; the availability of experienced and qualified technologists; and booking adequate time for imaging of difficult cases will significantly reduce the need for sedation in an imaging department.

21.3.3 Special Considerations in ^{18}F-FDG PET/CT

The use of PET/CT was less frequent than adults for several reasons, including the concern about the radiation dose, less common frequency of children malignancy, and the lack of availability of PET/CT in pediatric centers. However, the usefulness of PET/CT in pediatric malignancy has been shown in many studies during the last decade. Although the basis of PET/CT in children is the same as adult, there are some physiologic variation in ^{18}F-FDG biodistribution

and potential pitfalls in pediatric population which are needed to be addressed for correct interpretation of the images. Some of these issues are discussed in this section.

21.3.4 Isotopes and Radiopharmaceuticals

PET isotopes are generally cyclotron produced and have shorter half-lives than their conventional nuclear medicine counterparts. Fluorine 18 (F18), with a half-life of 110 min, is among the longer lived PET tracers. The most common F18 tracer is fluorodeoxyglucose (^{18}F-FDG). ^{18}F-FDG has found numerous applications in the assessment and staging of cancers throughout the body, assessing response to treatment, and is used widely in the assessment of organ metabolism particularly in the heart and brain.

F18′s half-life is long enough to permit off-site production and compounding into a radiopharmaceutical of interest. Other commonly used PET isotopes include N13 (half-life ~10 min) and O15 (half-life ~2 min) which are used in N13 ammonia and oxygen 15 water studies, respectively. The half-life of these isotopes is so short that they necessitate production in an on-site cyclotron. Such cyclotrons have dropped dramatically in price in recent years. Negative ion cyclotrons are entirely self-shielded and have a small footprint in an imaging department. On-site compounding and synthesis of PET tracers can be semiautomated but does usually require dedicated personnel including, ideally, a radiopharmacist.

21.3.5 Protocols for Fluorodeoxyglucose PET

As in adult, reviewing the history, clinical indication, history of diabetes, fasting states, recent infection, patient ability to lie still during the acquisition, and the need for sedation should be reviewed before the study [41]. Patients are instructed to fast and not consume beverages, except for water, for at least 4–6 h before the administration of ^{18}F-FDG to decrease physiologic glucose levels and to reduce serum insulin levels to near basal levels. Insulin levels greatly affect the biodistribution of ^{18}F-FDG, and where ^{18}F-FDG is used, care should be taken to ensure that a patient has not eaten in the 4–6 h preceding a study. Blood glucose should be checked before the administration of ^{18}F-FDG and should be in the range of approximately 3–11 μmol/mL. Diabetic children pose a special problem and may, if they are significantly hyperglycemic, administer a weight-based sliding scale dose of insulin and wait at least an hour prior to injection. It would be better to rebook the case if possible to a day when euglycemia is achieved. Weight, height, and blood glucose concentrations are recorded for all patients.

Image acquisition for the whole body PET scan usually starts approximately 60–90 min after injection of 5.18 MBq/kg (0.14 mCi/kg) ^{18}F-FDG, at doses ranging from 37 MBq (1 mCi) to 370 MBq (10 mCi). Patients were imaged from skull base to mid-thighs (approximately 3 min per bed position). The number of bed positions depends on the size of the patient, and it is usually less than 7 bed positions in small children and 7–10 bed positions for adolescents. In general, the arms are elevated over the head to avoid beam-hardening artifacts over the torso [41]. However, for optimal imaging of the head and neck, the arms should be positioned along the side [41]. The patient should void before the acquisition of the images to limit the radiation dose to the kidneys and bladder and also to be able to lie still on the bed for the acquisition time. Metallic objects and any other unnecessary objects should be removed from the patient whenever possible [41].

Dual-time point ^{18}F-FDG PET imaging usually consists of initial imaging at 60 min after tracer injection and then reimaging later at 2–4 h postinjection. Dual-time point image is based on the premise that ^{18}F-FDG uptake in inflammatory cells usually washes out, while ^{18}F-FDG tends to

be retained in malignant cells [42, 43]. Dual-time protocols have been used in pediatric population but for logistic reasons are not frequently applied in practice [44].

In children and adolescents and particularly when the weather is cold, it can be helpful to provide an ambient room for approximately 1 hour prior to injection of ^{18}F-FDG to decrease metabolism in brown fat [45]. Patients who had recently undergone diagnostic CT scans are imaged using a low-dose helical CT scan (in our protocol: 5 mm/slice, 90 kV; 20 and 30 mA for patients weighing <30 and ≥ 30 kg, respectively) prior to the PET scan for attenuation correction and anatomic localization. Diagnostic CT scans were obtained when clinically indicated and when patients do not have a recent CT scan. In those cases, the attenuation correction is calculated based on the correlative diagnostic CT images (in our protocol: 5 mm/slice, 120 kV, and a weight-based range for the mA, with dose modulation).

21.3.6 F18-FDG PET Normal Variants and Pitfalls in Children

The normal distribution of ^{18}F-FDG uptake in children is unique and may differ from that in adults. A number of physiologic variants are commonly seen, including normal physiologic activity in the head and neck, heart, breast, thymus, liver, spleen, gastrointestinal tract, genital system, urinary collecting system, bone marrow, muscles, and brown adipose tissue [46]. Benign lesions with increased ^{18}F-FDG activity are also frequently seen and can be misinterpreted as malignancies [46]. Other parameters such as the standardized uptake value (SUV) can also be different in pediatric population.

21.3.7 Standardized Uptake Values

The standardized uptake value (SUV) is a measurement unique to PET and is defined as attenuation-corrected activity in a region of interest divided by decay-corrected injected activity divided by body mass [47, 48]. It is also important to note that activity in a region of interest does change somewhat with different devices and reconstruction algorithms [49]. Still, standardized uptake value is the key semiquantitative parameter on which PET quantification is based and can be presumed to be reasonably reliable when patients are reimaged on the same device with the same dose of tracer over a time frame such that body weight is reasonably consistent.

SUVmax, or the largest SUV value in an ROI, is often chosen due to its reproducibility between readers (i.e., cancers are generally hotter on PET toward their center of mass, due to both cellular density and partial volume effects). Changes in SUV or SUVmax can indicate the aggressiveness of disease or response to therapy. In general, cancer responding to therapy will show a decrease in SUVmax, with the exception of radiation treatment of tumor which will often go through a short-term hypermetabolic phase followed by a gradual decline (see below). Measurement of SUV in small ROIs can be made less reliable by partial volume effects [50] (see Chap. 15 for further details).

It is important to recognize that fat has a relatively low metabolic rate, and so some authors prefer to normalize to lean body mass or body surface area in the SUV calculation, particularly in obese patients, where normalized to body weight SUV can be artifactually overestimated in non-adipose tissue [48]. The percentage of fat is changing in pediatric patients from 11 % in the newborn to about 26 % during the following 5 months and then decreases gradually until 12 months of age [51]. After that the percentage of fat depends on many factors including diet, physical activity, and genetics [51]. Thus, pediatric SUV normalized to body weight is not exactly the same as that of adults. Moreover, the clinical significance of SUV values in different pathologies and normal versus suspected malignancy reference numbers in children cannot be simply

extrapolated from the adult values and should be interpreted cautiously. The optimal method for calculating SUV in children may be different from that used in adults due to the body changes and growth that take place during childhood. Therefore, it has been suggested that, in pediatric patients, SUV calculated on the basis of body surface area would serve as a better metabolic activity marker than would SUV calculated on the basis of body weight.

21.3.8 Thymus

Thymic tissue persists in children and often persists into early adulthood. Thymus is often mildly to moderately ^{18}F-FDG avid on PET and can be mistaken for mediastinal tumor (Fig. 21.1). Thickness of the thymus gland, measured perpendicular to a lobe, should be less than 1.8 cm in children under twenty and 1.3 cm in older patients [52, 53]. The shape of the thymus is quadrilateral during childhood and triangular during adolescence. Morphologic features such as thickness of the gland and its homogeneity are used on either diagnostic or low-dose localizer CT to determine the presence of disease [53].

Thymus uptake of ^{18}F-FDG can increase following chemotherapy which is a frequent consequence of chemotherapy, especially in young patients undergoing chemotherapy for lymphoma, leukemia, or testicular cancer. The reasons for this hyperplasia are debated. An important function of the thymus is to "train" lymphocytes toward adap-

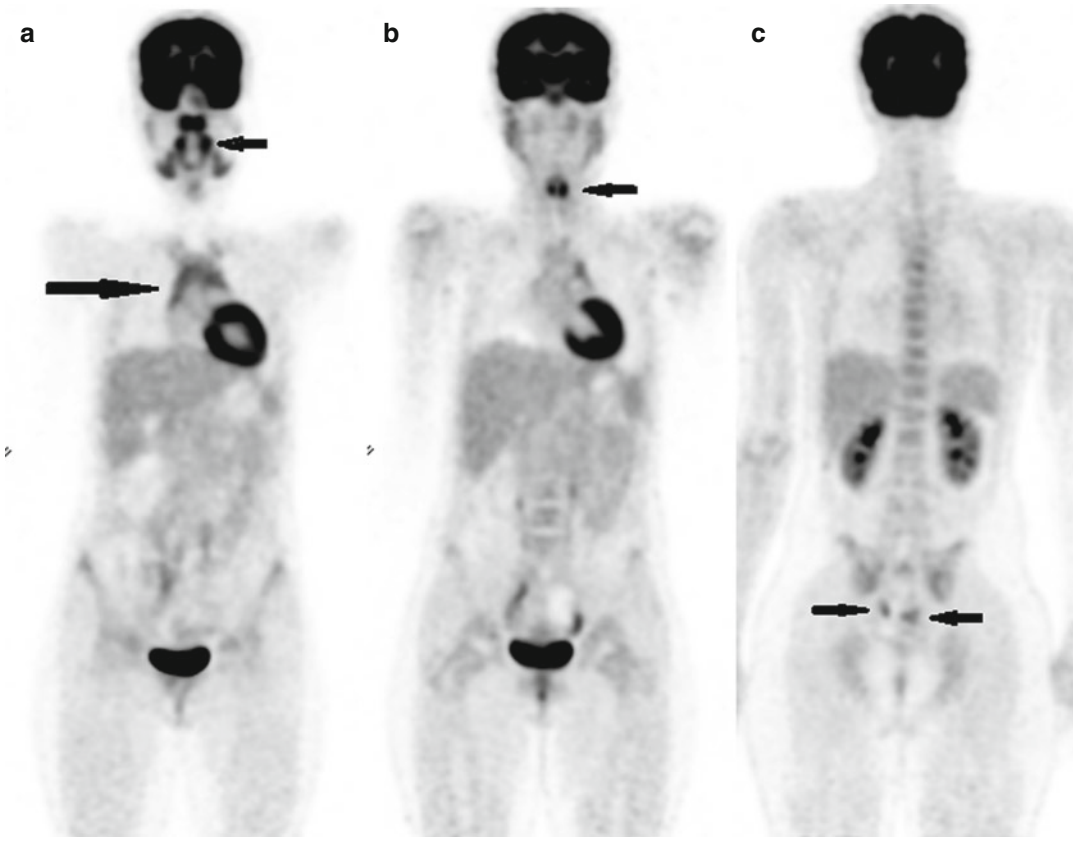

Fig. 21.1 Physiologic activity in a 13-year-old female. (**a**) Physiologic activity in the palatine and lingual (*small arrow*) tonsils and normal uptake in the thymus (*long arrow*). (**b**) Physiologic activity in the vocal cords or muscles in the vocal cord region (*arrow*). (**c**) Normal uptake of the bone marrow. Foci of activity in the pelvic region due to follicular activity of ovaries (*arrows*)

tive immunity. Chemotherapy is associated with decreased white counts and thymus atrophy. Steroids, frequently concomitant with chemotherapy for the treatment of lymphoma, can also induce thymus atrophy which then "rebounds" with subsequent marrow hyperplasia [54].

It can be challenging to differentiate benign from malignant thymus ^{18}F-FDG activity. In general, homogeneous thymic uptake at post-therapy ^{18}F-FDG PET and the absence of uptake at pre-therapy ^{18}F-FDG PET indicate post-therapy thymic hyperplasia. To some extent the SUV of thymus tissue can guide decisions. Brink et al. reported a mean SUV of 2.8 and max of 3.8 in thymic hyperplasia [54]. Ferdinand et al. indicates that thymic SUV >4 warrants further investigation to exclude malignancy [55].

Thymic carcinoma is a rare malignancy in children and in general is associated with significantly increased ^{18}F-FDG uptake. Sasaki et al. reported SUV of 7.2 ± 2.9 in thymus carcinoma, which is in turn significantly higher than activity found in invasive thymoma (3.8 ± 1.3) and noninvasive thymoma (3 ± 1) [56]. Thymoma can therefore not be reliably differentiated from thymus hyperplasia. Morphologic features on CT are helpful in these cases to differentiate benign change from malignancy.

21.3.9 Tonsils

The tonsils are very metabolically active in children and can demonstrate significant ^{18}F-FDG avidity on PET scan (Fig. 21.1). The palatine and lingual tonsils, in part because of their size, are particularly avid. Upper respiratory tract infections can cause tonsillar hypertrophy and increased thymus metabolism. The symmetry of tonsil activity is an important means of differentiating benign from malignant processes [57]. Lymphoma in the head and neck, oropharyngeal malignancy, and posttransplant lymphoproliferative disorder (PTLD) are all associated with increased ^{18}F-FDG activity and can mimic or be difficult to differentiate from normal functioning tonsillar tissue. Comparison to any prior ^{18}F-FDG PET imaging and correlation to CT, ultrasound, or MR imaging can be helpful in the assessment of challenging cases.

21.3.10 Marrow Hyperplasia

Marrow suppression is a frequent complication of chemotherapy with or without colony-stimulating factor administration and can also result from tumor infiltration of bone marrow. After treatment, most often by chemotherapy or steroids, suppressed marrow can subsequently rebound and demonstrate diffuse hypermetabolism, with increased activity on ^{18}F-FDG PET that can be confused for diffuse malignant change [58–60]. Anemia, including thalassemia, medications such as interferon can also cause diffuse increased bone activity and represent an important cause of false-positive findings [61, 62]. Treatment with hematopoietic cytokines such as granulocyte colony-stimulating factor (CSF), hematopoietic growth factor, or erythropoietin can also produce diffuse skeletal ^{18}F-FDG accumulation. Increased activity can persist for up to 3 weeks after the discontinuation of granulocyte CSF treatment. Increased activity in the spleen is also frequently noted in association with increased marrow activity (Fig. 21.2). Normal bone marrow is mildly ^{18}F-FDG avid that is less intense than liver activity (Fig. 21.1).

21.3.11 Brown Fat

Physiologic high uptake from activated adrenergic innervation of adipocytes is a normal variant especially in children. This brown fat, rich in mitochondria, is more common in children than adults and is typically found in the neck, supraclavicular regions, axillae, mediastinum, and paravertebral and perinephric regions. The distribution of brown fat is usually symmetric. However, focal and asymmetric uptake can occur in the neck or mediastinum, leading to false-positive results.

Brown fat because of its ^{18}F-FDG avidity can present a considerable problem in the interpretation

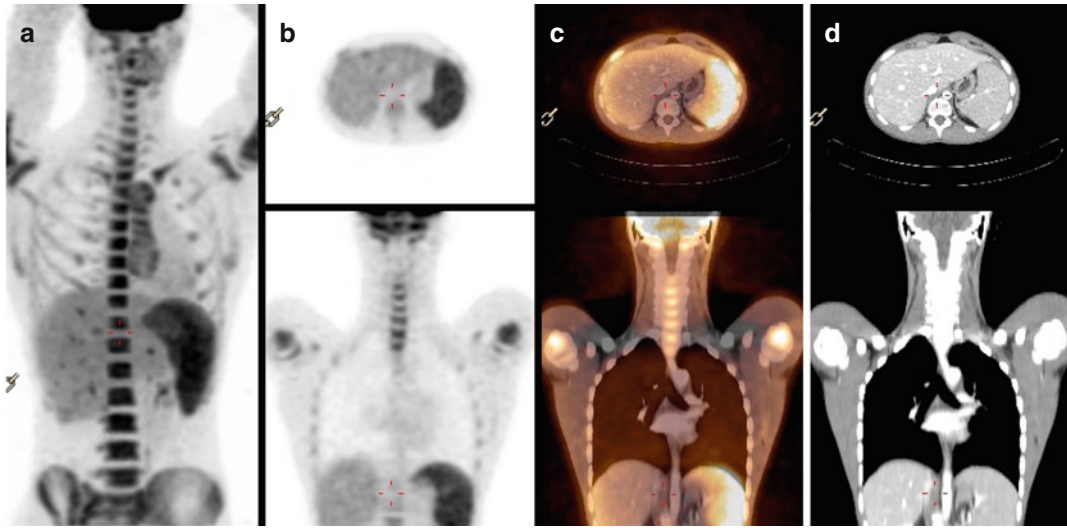

Fig. 21.2 18F-FDG PET/CT in a 17-year-old patient with lymphoma after two cycles of chemotherapy and one day after injection of GCSF. (**a**) Maximum intensity projection (MIP), (**b**) Axial and coronal PET, (**c**) Axial- and coronal-fused PET/CT, and (**d**) CT scan showed marked improvement of the activity previously visualized in the mediastinum (not shown here). Increased activity in the spleen and bone marrow is due to GCSF effect

of ^{18}F-FDG PET studies (Fig. 21.3). The most practical way to control brown fat activity is to control the temperature of the patient before injection and in the period between injection and image acquisition [45, 63]. Some authors have also used medication, most commonly propranolol and diazepam, to decrease activity in brown fat [63].

Fusion imaging with CT enables to differentiate between ^{18}F-FDG uptake corresponding to fat-attenuation tissue at CT and uptake from pathologic causes.

21.3.12 Posttreatment Change

It is generally recommended to wait at least 4–6 weeks after surgery and at least 1–2 weeks after biopsy prior to performing ^{18}F-FDG PET [64]. A shorter interval than this has been associated with physiologic increased uptake in healing tissues which could be mistaken for a false positive. It is important for institutions to develop a practice pattern in conjunction with the treating physician.

Radiation therapy is associated with inflammation and the recruitment of white blood cells which are intensely ^{18}F-FDG avid. Thus, tumors subjected to radiotherapy can demonstrate marked increased ^{18}F-FDG uptake which can persist for weeks. It is ideal to wait 6 weeks after radiation therapy prior to PET imaging to assess response [64]. Reduced bone marrow ^{18}F-FDG uptake can be noted several months after external beam radiation therapy. This phenomenon has been attributed to the replacement of bone marrow by fatty tissue.

21.3.13 Other Pitfalls

If children are significantly active before ^{18}F-FDG administration or in the interval between ^{18}F-FDG administration and imaging, uptake in metabolically active muscles may limit assessment. It is best for patients undergoing ^{18}F-FDG PET imaging to avoid strenuous exercise or vigorous sports in the days which precede imaging. Chewing of gum or sucking pacifier after ^{18}F-FDG injection can cause symmetric intense uptake in the masseter muscles. Uptake in the diaphragm, the crura of the diaphragm, and the intercostal muscles can be detected in children who have been crying during the uptake phase.

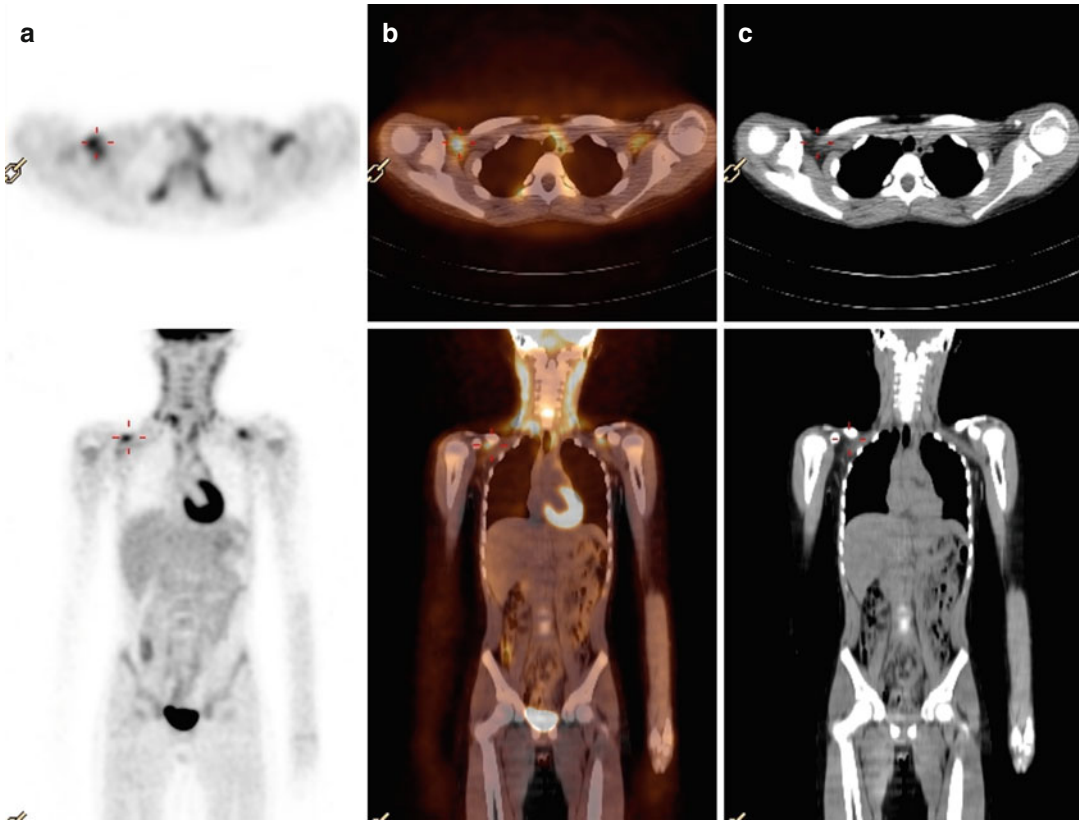

Fig. 21.3 Axial and coronal PET (**a**), fused PET/CT (**b**), and CT (**c**) of 18F-FDG PET/CT in a 12-year-old boy diagnosed with large B-cell lymphoma 3 years before, referred for evaluation of recurrence. Multiple foci of FDG activity are noted in the neck, supraclavicular region, and chest bilaterally corresponding to the hypodense regions on CT due to brown fat uptake. The patient had positive neck lymph nodes, an FDG-avid lesion in the right lung, and lumbar spine involvement which were not shown here

A common source of a false negative in ^{18}F-FDG PET scan is altered biodistribution caused by improper patient preparation. Usually this is due to increased circulating insulin and characterized by decreased uptake in tumor, decreased uptake in the brain, and increased uptake in peripheral skeletal muscle. Repeating the exam may be indicated in such a situation [72].

A second common cause of a false negative is the collision of tumor activity with the normal biodistribution of activity and can be a problem particularly in the genitourinary system on ^{18}F-FDG PET as ^{18}F-FDG is cleared by the kidneys [72]. Visibility of cancers in the genitourinary tract can be limited on ^{18}F-FDG PET. If possible and age appropriate, patients should empty the bladder prior to ^{18}F-FDG PET image acquisition.

21.3.14 Other Radiopharmaceuticals

Studies on the use of other PET tracers beyond ^{18}F-FDG in pediatric population are limited. ^{18}F-sodium fluoride (^{18}F-NaF) has been extensively used in adult for detection of bone metastases in different tumors and can also potentially be useful in pediatric patients [65, 66]. Accumulation of ^{18}F-NaF in the skeletal system is similar to that of 99mTC-MDP based on local blood flow and osteoblastic activity. However, the protein binding is lower allowing for earlier images than conventional bone scan. The extraction of ^{18}F-NaF is also higher than 99mTC-MDP. Thus the image contrast is better with ^{18}F-NaF. PET images also provide better spatial

resolution than conventional gamma cameras. However, the radiation dose is higher than the bone scan. The recommended dose of ^{18}F-NaF is approximately 2.2 MBq/kg, with a minimum of 11.1 MBq and a maximum of 148 MBq [67]. Imaging starts 45–60 min after the radiotracer administration. The biodistribution of the tracer is similar to the 99mTC-MDP and depends on the patient's age with more activity in the growth plates.

3′-Deoxy-3′-[F18]-fluorothymidine (^{18}F-FLT) FLT is an analog of thymidine and the uptake reflects cellular proliferation. Thus increased activity with ^{18}F-FLT is more suggestive of tumor proliferation than inflammation. FLT is retained in proliferating tissues and malignant tumors through the activity of thymidine kinase 1 (TK1), an enzyme that is highly expressed during the DNA synthesis phase of the cell cycle [68]. TK1 phosphorylates FLT to form negatively charged FLT-monophosphates which are impermeable to the cell membrane. Since most tumor cells have a much higher TK1 activity than normal cells, the intracellular trapping of FLT and accumulation of radioactivity occurs [68]. Current published literature have demonstrated the feasibility of using FLT PET imaging in patients with lung cancer [69–72], gastrointestinal cancer [73, 74], melanoma [75], lymphoma [76, 77], breast cancer [78, 79], soft tissue sarcomas [80], as well as primary malignant brain tumors in adults and children [81–85]. ^{18}F-FLT has been safely administered to children between the ages of 2–13 years with no observable adverse effects [81–85]. ^{18}F-FLT minimally crosses intact blood–brain barrier [86, 87], thus the high background activity which is typically visualized with ^{18}F-FDG is not seen using ^{18}F-FLT. Published literature related to the use of ^{18}F-FLT PET in the evaluation of CNS tumors in the pediatric population is limited and restricted only to studies involving children with glioblastoma [81–85]. The recommended dose is 5.18 MBq/kg (0.14 mCi/kg) using a minimum dose of 37 MBq (1 mCi) up to a maximum of 370 MBq (10 mCi). Imaging is usually performed 45–60 min after the radiotracer administration.

Tumors have varying degrees of hypoxia. Tumor hypoxia may be related to chaotic vasculature in some tumors or rapid growth in others. It is usually associated with increase angiogenesis and tumor aggressiveness [88, 89]. Studies have shown that tumor hypoxia increases the risk of metastases and decreases the sensitivity to chemo/radiation therapy [90–93]. This may be due to the aggressiveness of the tumor or abnormal vasculature that may diminish delivery of anticancer therapy. Using hypoxia-selective cytotoxins may increase the effect of chemo/radiation therapy [94–97]. Tumor hypoxia has been also reported to be associated with increased risk of recurrence and a poorer prognosis [89, 98]. Detection of hypoxic components of tumors is possible with histologic evaluation. However, due to the patient situation, tumor type, location, etc., surgical resection of tumors is not recommended in all malignancies. Moreover, in some instances, information of hypoxic component of tumor is needed before the surgical resection (e.g., before neoadjuvant treatment in osteosarcoma). Tissue biopsy is inaccurate in these situations since it may not reflect the whole tumor. Imaging is a surrogate marker of histological assessment to detect these hypoxic components as it is noninvasive and repeatable and represents the whole tumor. 1-α-D-(5-deoxy-5-[18 F]-fluoroarabinofuranosyl)-2-nitroimidazole (^{18}F-FAZA) is a 2-nitroimidazole-based molecule that undergoes reductive metabolism under hypoxic conditions, producing reactive intermediates that bind to intracellular macromolecules. Studies in adult population and different tumors have shown that 18F-FAZA is a promising radiotracer for detection of hypoxic components in tumors [96, 99]. The recommended dose is 5.2 MBq/kg (0.14 mCi/kg) using a minimum dose of 37 MBq (1 mCi) up to a maximum of 370 MBq (10 mCi). Imaging is usually performed 2–3 h after the radiotracer administration (hypoxia tracers are reviewed in Chap. 17).

11C-Methionine (11C-METH) is an amino acid PET tracer mainly used in brain imaging tumors. The uptake in brain tumor is probably related to passive diffusion from the altered blood–brain barrier and active uptake by the

tumor due to increased amino acid metabolism. Similar to the ^{18}F-FLT, the background activity is very minimal with 11C-METH, allowing detection of small viable brain tumors. The pediatric studies were limited; however, they showed a higher sensitivity of 11C-METH for the detection of viable brain tumor than that of ^{18}F-FDG [100, 101]. The pediatric dose and protocol are not well established. In general, due to the short half-life of C11, imaging will start 20 min after the administration of 5.5 MBq/kg of the radiotracer [101].

68Ga-DOTA-conjugated peptides [68Ga-DOTA0-Tyr3]octreotide (68Ga-DOTATOC, 68Ga-edotreotide), [68Ga-DOTA0-1NaI3]octreotide (68GaDOTA-NOC), and [68Ga-DOTA0 -Tyr3]octreotate (68GaDOTA-TATE) have been used to detect somatostatin receptor-positive tumors. Somatostatin receptors are positive in a variety of tumors [102]. The activity administered ranges from 100 to 200 MBq in adults [102]. The exact dose in pediatric patients is not well established; the dose in children should be reduced according to the recommendations of the EANM Paediatric Task Group [102]. Imaging is usually obtained 45–90 min after the radiotracer administration depending on the type of analog used [102].

Other radiotracers like 11C-hydroxyephedrine (HED), 11C-epinephrine, and 18-F-dihydroxyphenylalanine (DOPA) have been also used for sympathetic nervous system and neuroendocrine tumors. 11C-HED is similar to norepinephrine (NE), but unlike NE it is not metabolized and is used for sympathetic nervous tumors imaging [103]. 11C-Epinephrine has been used in pheochromocytoma and neuroblastoma [104]. ^{18}F-DOPA has been also used in pheochromocytoma, hyperinsulinemia, and brain tumors [105].

21.4 Image Fusion

Nuclear medicine image techniques benefit strongly from attenuation correction to mitigate the effects of photon absorption by the patient. Although historically transmission attenuation correction was used for this purpose [106], the widespread dissemination and reduced cost of CT led to the coupling of PET and SPECT to low-dose CT exams for anatomic localization and correction. Attenuation, itself a function of density, is ideally corrected by the density maps produced in CT. Acquisition of CT data with PET data usually minimizes the registration problem.

Increasingly in pediatric nuclear medicine practice, where a diagnostic CT is required, PET imaging can be acquired simultaneously with diagnostic CT on a hybrid device supporting a multi-slice CT scanner [107]. PET/MRI is a more recent development which enables the simultaneous acquisition of PET and MRI data, though at considerable expense and with potentially longer acquisition times. Pediatric centers, which usually have to sedate children undergoing MRI [108], often cite both this fact and the limitations of MRI for attenuation correction as a reason not to opt for a hybrid PET/MRI device. Using multisequence MRI to perform attenuation correction reliably is an area of active investigation, and significant advances have been recently made [109–112].

21.5 Tumors of the Sympathetic Nervous System

21.5.1 Neuroblastoma

Sympathetic nervous system (SNS) tumors account for about 7 % of all pediatric malignancies. Neuroblastoma, including ganglioneuroblastoma, is the most common form of all SNS tumors in children (approximately 97 %). Neuroblastoma (NBL) is a common lesion in young children and unfortunately associated with significant mortality. NBL accounts for 20 % of malignancy in children diagnosed below the age of 1 year and is especially common during the first 3 months of infancy. NBL is the second most common, after brain tumors, solid malignancy in childhood.

The long-term survival of NBL patients remains challenging. Age remains among the most important predictors of survival in NBL

patients, with presentation beyond 5 years associated with a 5-year survival of approximately 40 %. Survival in younger children, especially less than 1 year, has improved dramatically since 1975, from approximately 35–83 % today as a result of improved therapy. Aside from age, stage at diagnosis is a very important prognostic indicator, with complete resection of a local tumor and negative margins indicating a more optimistic long-term prognosis. Molecular and cytogenetic factors including DNA content, proto-oncogenes, and catecholamine synthesis are all linked to prognosis.

The etiology of neuroblastoma is unclear. The predilection of the tumor in infants has implicated genetic factors or in utero toxicity, for example, alcohol [113] or other drug exposure, as potentially playing a role in causation [114, 115]. The effects of maternal substance and/or environmental exposures on the development of neuroblastoma is however controversial [116].

Diagnosis of neuroblastoma is usually enabled by a combination of imaging findings and elevated serum or urine catecholamines. There is a spectrum of catecholamine metabolites including dopamine, homovanillic acid, and vanillylmandelic acid which can be represented in neuroblastoma patients [117].

The natural history of neuroblastoma is quite variable, with some patients demonstrating spontaneous regression and some patients demonstrating differentiation of tumor into mature nonmalignant tissue. Other NBLs demonstrate aggressive behavior despite multimodality treatment and are associated with poor outcomes.

The International Neuroblastoma Staging System (INSS) uses the distribution of disease as evidenced by imaging studies, operability, lymph node metastases, and bone marrow metastases as factors influencing prognosis (Table 21.2). The more recent International Neuroblastoma Risk Group (INRG) system describes 13 potential prognostic factors to categorize patients into four groups (5-year survival of <50 %, 50–75 %, 75–85 %, and >85 %) [118].

Metastases are unfortunately common at presentation, and hence multimodality imaging is important in the initial assessment of neuroblastoma [119]. Ultrasound is a frequent first test in a child with typical symptoms of abdominal mass, pain, anemia, fever, weight loss, paraneoplastic syndrome, and occasionally blindness. Ultrasound is usually followed by diagnostic CT or MRI. With positive biochemistry, scintigraphy is generally employed I123 MIBG for definitive workup [120, 121].

Table 21.2 International Neuroblastoma Staging System (INSS)

Stage	Description
1	Localized tumor with complete gross excision (with or without microscopic residual disease) with no ipsilateral lymph nodes involvement
2a	Localized tumor with incomplete gross excision and no ipsilateral lymph involvement
2b	Localized tumor with or without complete gross excision, with ipsilateral lymph nodes involvement
3	Unresectable unilateral tumor crossing the midline (with or without regional lymph node involvement); or localized unilateral tumor with contralateral regional lymph node involvement; or midline tumor with bilateral extension which is unresectable or with positive lymph nodes
4	Any primary tumor with involvement of distant lymph nodes, bone, bone marrow, liver, skin, and/or other organs (except as defined for stage 4S)
4s	Localized primary tumor (as defined for stage 1, 2A, or 2B), with metastases limited to the skin, liver, and/or bone marrow (limited to infants 1 year of age)

MIBG scintigraphy has been extensively described for the workup of NBL and remains standard of care at even quaternary pediatric oncology centers [120, 121]. MIBG has been used in prognostication and in assessment of response to therapy, with a decrease or absence of MIBG activity following therapy indicative of a good prognosis. Similarly, as bone metastases are quite common in NBL, the Tc 99m MDP bone scan has been used extensively for the assessment of osseous metastases [122]. However, in approximately 10 % of cases, NBL is not MIBG avid (Fig. 21.4).

^{18}F – FDG PET has shown utility in NBL patients, and both the primary tumor and metastases may be ^{18}F-FDG avid (Fig. 21.5), even in

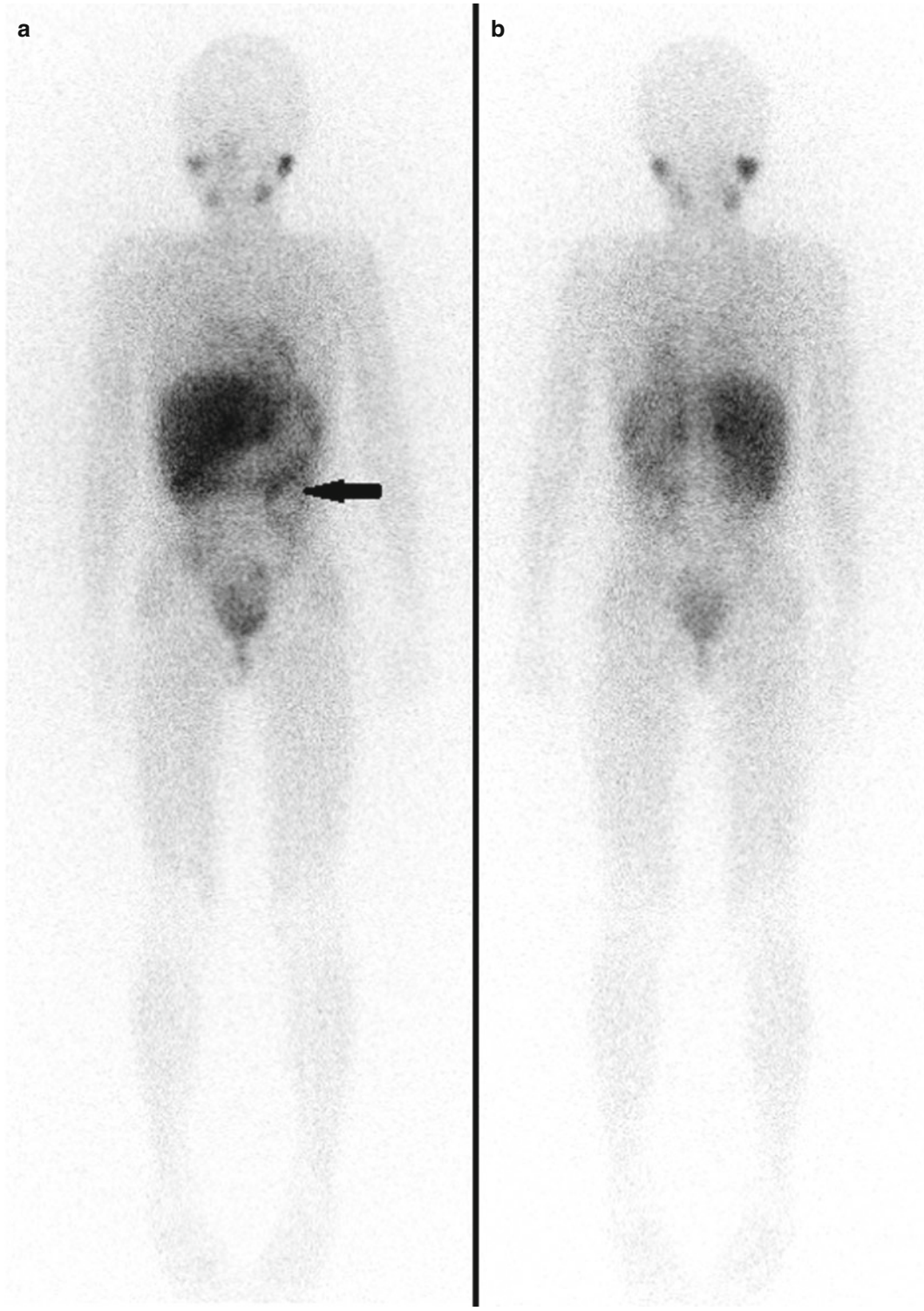

Fig. 21.4 Twelve-year-old male with neuroblastoma in the left abdomen. (**a**) Anterior and (**b**) posterior MIBG scan showed mild MIBG activity in the region of the tumor (*arrow*). The liver uptake was inhomogeneous with no definite focal increased activity

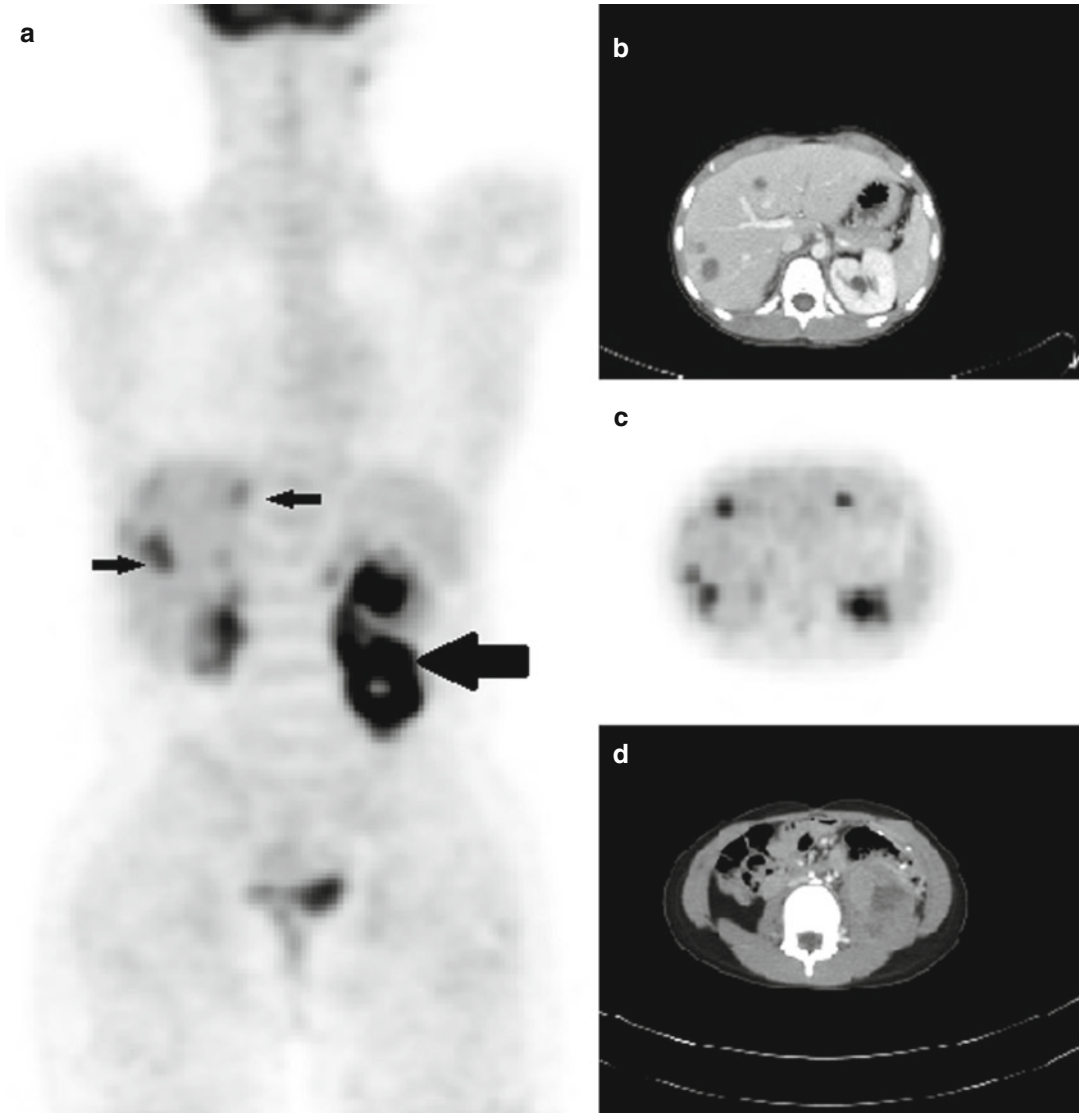

Fig. 21.5 18F-FDG PET/CT in the same patient as described in Fig. 21.3, with a left paravertebral mass with very mild MIBG uptake. (**a**) Coronal PET showed a heterogenous intense uptake in the left abdominal paravertebral lesion as well as multiple foci of increased activity in the liver suggestive of metastases. A superimposed infectious process in the liver could not be excluded. Biopsy proved the diagnosis of metastatic neuroblastoma. (**b**) Axial CT from the upper abdomen and (**c**) axial PET showed multiple lesions in the liver. (**d**) Axial CT from the abdomen shows the left abdominal paravertebral mass

occasional MIBG-negative NBL. A study of 60 patients by Sharp et al. comparing ^{18}F-FDG to I123 MIBG documented the superiority of ^{18}F-FDG for early-stage disease and the potential benefits of MIBG for evaluation of higher-stage disease [123]. MIBG demonstrated superiority for the evaluation of stage 4 disease. In addition, ^{18}F-FDG can provide helpful information in cases of mildly MIBG avid tumor at major decision points in therapy, such as prior to bone marrow transplantation or major surgery (Figs. 21.4 and 21.5). ^{18}F-FDG is advantageous in that the test can be performed in one day. The other benefits of ^{18}F-FDG are the higher photon energy and the

better attenuation correction characteristics of PET in abdominal imaging, especially in obese patients. In another study by Choi et al. on 30 neuroblastoma patients, ^{18}F-FDG PET was more sensitive than CT in the evaluation of distant lymph node involvement [124].

$^{18}\mathrm{F-FDG}$ does however have important caveats. Firstly, ^{18}F-FDG can be a nonspecific tracer, showing uptake in inflammatory lesions or any of the false positives indicated above. Secondly, ^{18}F-FDG has been shown to be less useful than MIBG for the evaluation of osseous/bone marrow disease [123]. There is some evidence however that ^{18}F-FDG can have better accuracy for the detection of soft tissue metastases than MIBG [103, 125]. Thus, until larger studies can be performed, ^{18}F-FDG and MIBG are perhaps best considered complimentary tools in NBL.

11C-Hydroxyephedrine, the PET equivalent of MIBG, has been used in a small number of patients and was found to be comparable though potentially limited in the assessment of perihepatic disease due to high background activity in the liver on hydroxyephedrine PET [103]. ^{18}F-FDOPA is another tracer which has shown considerable promise in NBL, with Piccardo et al. showing higher sensitivity in FDOPA compared to paired I123 MIBG in 28 scans over 19 patients [126]. FDOPA detected distant lesions in 94 % of cases rather than 65 % of cases with MIBG. Management was hence changed in 9/28 or 32 % of scans.

NBL does demonstrate somatostatin receptors and hence gallium 68 DOTA is of potential in PET imaging. Ga 68 DOTATOC has been shown to be superior to planar indium 111 octreotide in a series of neuroendocrine tumors [127]. In a small series, Ga 68 DOTATOC PET was found to have a sensitivity (97.2 %) superior to MIBG (90.7 %) [128], a result which will hopefully be confirmed in a larger study.

21.5.2 Pheochromocytoma

The pheochromocytoma arises from chromatin cells of the adrenal medulla or, occasionally, from extra-adrenal paraganglionic tissue. Approximately 85 % of cases arise from the adrenal medulla. The organ of Zuckerkandl and ganglionic tissue surrounding the kidney can also give rise to pheochromocytoma. The pheochromocytoma is much more common in adolescents than children, with 11 years being the mean age of presentation.

When pheochromocytoma arises in children, it is often in association with a genetic syndrome, most commonly von Hippel–Lindau, multiple endocrine neoplasia, neurofibromatosis 1, and familial paraganglioma syndrome [129, 130]. Thus, the presentation of a child with pheochromocytoma should prompt further investigation for other abnormalities within the spectrum of these syndromes and might include further imaging of the head, thyroid, skeleton, and abdomen [130, 131].

Elevated levels of circulating plasma catecholamines or urine catecholamines in the correct clinical presentation are essentially diagnostic [132]. Paraganglioma, conversely, is less likely to be associated with biochemical abnormality, and so in syndromes where both pheochromocytoma and paraganglioma may be present, a negative serum or urine catecholamine level should not dissuade from further imaging including imaging of the sympathetic nervous system [131].

Ultrasound, CT, and/or MRI is often employed in the initial evaluation of pheochromocytoma, with signal and enhancement characteristics of the latter being essentially diagnostic in the correct clinical and biochemical context [131]. MIBG imaging, usually bound to I123, confirms the diagnosis and is used to evaluate for any additional sites of involvement or distant metastatic disease [133]. Approximately 90 % of pheochromocytomas are MIBG avid.

Although pheochromocytoma is usually ^{18}F-FDG avid (Fig. 21.6), some lesions will not accumulate ^{18}F-FDG, and hence where PET is performed, an adrenergic PET imaging agent such as 11C hydroxyephedrine may be preferable where available to a glucose analog [134]. Pheochromocytomas frequently express somatostatin receptors and thus excellent preliminary results have also been obtained with gallium 68 DOTA somatostatin analogs in a limited literature [135].

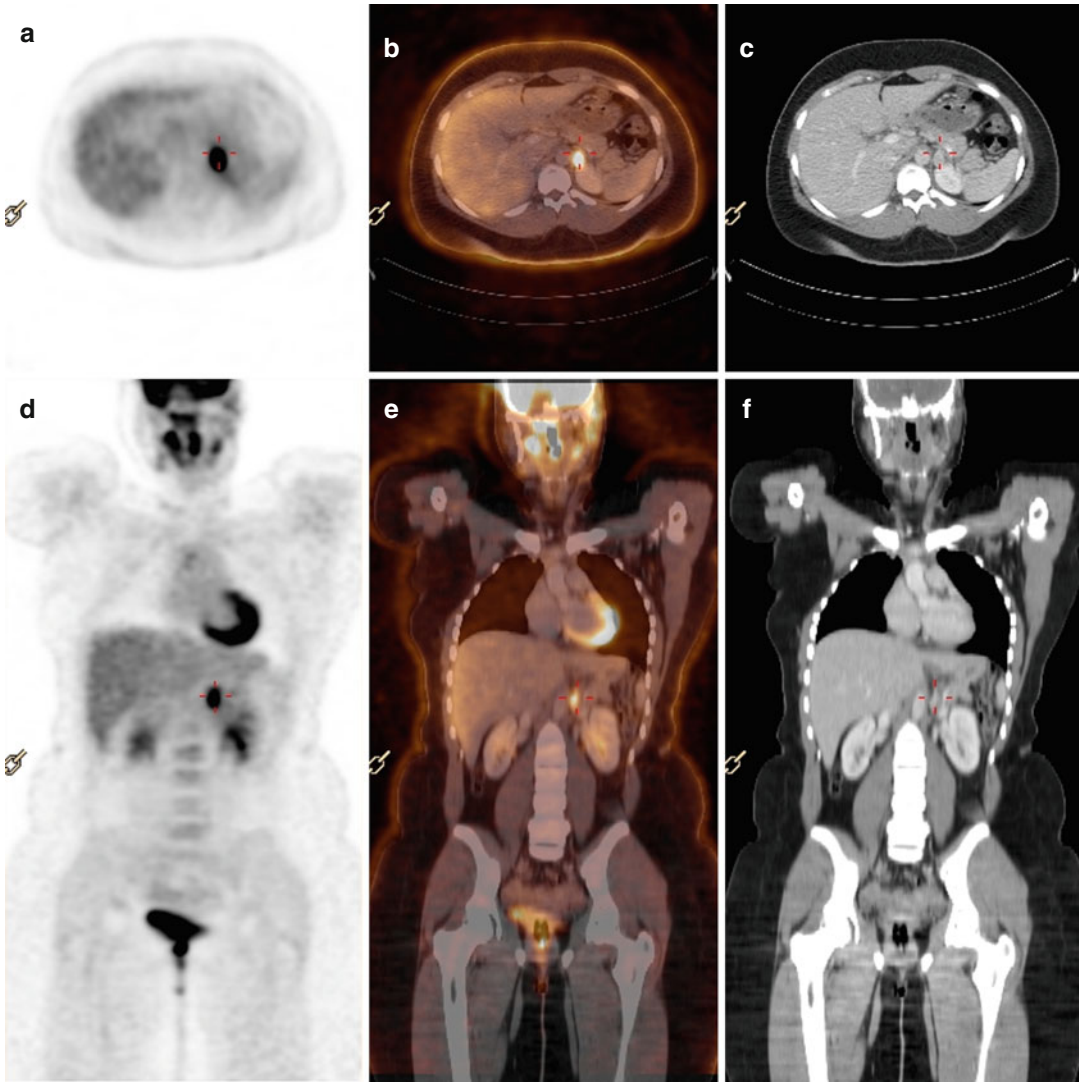

Fig. 21.6 Axial PET (**a**), fused PET/CT (**b**), and CT (**c**), coronal PET (**d**), fused PET/CT (**e**), and CT (**f**) of 18F-FDG PET/CT in an 18-year-old female, clinically and biochemically suspicious for recurrence or metastases of pheochromocytoma. Right suprarenal pheochromocytoma was resected a year ago. A focal intense FDG activity is noted in the left suprarenal region corresponding to the soft tissue density on the CT suggestive of pheochromocytoma. No other FDG-avid lesions were detected to suggest metastasis

21.6 Lymphoma

Lymphoma is the third most common type of childhood malignancy after leukemia and brain tumors, accounting for approximately 15 % of pediatric cancers. The peak age is 15–19 years old. Lymphoma makes up almost 24 % of the childhood malignancy for the age 15–19, while it accounts only 3 % of the pediatric cancers below the age of 5. Lymphoma is categorized into Hodgkin's disease (HD) and non-Hodgkin's lymphomas (NHL).

21.6.1 Hodgkin's Disease

HD is more common in young adults. It is more common in 15–30 years of age. The other peak age for HD is >55 years old. The 5-year survival

is more than 90 % for the patient younger than 20 years old. The exact etiology of HL is not well known. Both genetic predisposition and environmental factor (prior viral infection) have been suggested to be responsible for HD. According to the Revised European–American Lymphoma Update of the WHO classification, HD is categorized into two main groups: (1) nodular lymphocyte predominant Hodgkin's lymphoma (NLPHL) and (2) classical HD.

NLPHL accounts for approximately 10 % of all HD and has a very good prognosis. It frequently involves the cervical and axillary lymph nodes; mediastinal and extra-nodal involvements are rare. Classical HD is categorized into four histologic subtypes:

1. Nodular sclerosis: the most common type in North America and Western Europe; approximately 70 % of cases, with good prognosis
2. Mixed cellularity: the second most common in North America and Western Europe and probably most common in underdeveloped areas; characterized by pleomorphic cellular infiltrate of plasma cells, eosinophils, lymphocytes, histiocytes, and Reed–Sternberg cells; has intermediate prognosis
3. Lymphocyte rich: characterized by small lymphocytes with occasional and probably atypical form of Reed–Sternberg cells (lymphocytic–histiocytic); has a good prognosis
4. Lymphocyte depleted: rare in children; more common in HIV patient and positive EBV; has the worst prognosis

21.6.2 Non-Hodgkin's Lymphoma

NHL is more common in younger children. The 5-year survival is approximately 72 %. The incidence of NHL is less variable with age in children comparing with HD. Congenital immunodeficiency disorders (CIDs) and HIV are reported to be associated with an increased risk of NHL. NHLs are a heterogeneous group of disease, usually with higher proliferative neoplastic cells and aggressive behavior compared with the HD [136]. NHL can be categorized into many subgroups. The major subgroups are:

1. Burkitt and Burkitt-like lymphomas (more common in 5–14 years old; often occur in the abdomen)
2. Lymphoblastic lymphoma precursor T (usually mediastinal)
3. Anaplastic large cell lymphoma
4. Diffuse large B-cell lymphoma (DLBCL; most common subtype among 15–19-year-olds)
5. Follicular lymphoma

The NHLs can also categorize into slow-growing types (e.g., follicular lymphoma), more aggressive types (e.g., DLBC), and fast-growing types (e.g., Burkitt and Burkitt-like lymphomas).

The clinical presentation varies and depends on the type of lymphoma, location, and systemic presentations. Peripheral lymphadenopathy is the most common finding. Cough or shortness of breath secondary to the mediastinal mass, B symptoms (fever, weight loss, anorexia, and night sweats), tiredness, pruritus, neurologic symptoms, anemia, and bone pain are other sign and symptoms. Clinical history, physical examination, laboratory tests, chest X-ray, and CT scans are among the initial evaluation. Histopathology will confirm the diagnosis. Accurate staging of disease is important for prognosis and treatment management. On one hand, it is necessary to use appropriate intensive chemotherapy and radiotherapy (especially for HD) to achieve a good response, and on the other hand, it is essential to avoid unnecessary treatment to minimize the complications of therapy [137, 138]. For HD, Ann Arbor staging or Cotswold classification (a modification of Ann Arbor) is usually used, and for NHLs of the children, St. Jude Children's Research Hospital is the preferred staging system (Tables 21.3 and 21.4).

Nuclear medicine has an important role in evaluation of lymphoma. Bone scan with ^{99m}Tc-MDP is useful in detection of bone metastasis especially in HD. 67Ga citrate scan has been used for a long time as functional imaging modality for the staging and response to therapy with a

sensitivity and specificity of approximately 80 % and 90 %, respectively [139]. ^{67}Ga scan is more positive in high-grade B-cell or Burkitt lymphoma [140]. Due to increased radiation exposure, lower resolution, and the need to image the patient for a longer time, ^{67}Ga scan has been replaced by ^{18}F-FDG PET/CT for initial staging and evaluation of response and recurrence in children.

Table 21.3 Hodgkin's disease staging

Stage	Description
Stage I	A single lymph node group involvement or localized involvement of an extralymphatic organ
Stage II	More than one lymph node group involvement or localized involvement of an extralymphatic organ (all on the same side of the diaphragm)
Stage III	Involvement of lymph nodes on both sides of the diaphragm with or without localized involvement of an extralymphatic organ
Stage IV	Diffuse involvement of one or more extralymphatic organs

Table 21.4 St. Jude's staging for childhood NHL staging

Stage	Description
Stage I	Single tumor outside the lymph nodes or nodal involvement in one group of lymph nodes (not in the mediastinum or abdomen)
Stage II	A single extra-nodal tumor with regional node involvement
	More than one group of nodes on the same side of the diaphragm
	Two extra-nodal tumors on the same side of the diaphragm
	A primary gastrointestinal tract tumor with or without involvement of associated mesenteric nodes and can be completely resected by surgery
Stage III	Two single extra-nodal tumors or two or more nodal groups on the opposite sides of the diaphragm
	All the primary chest tumors
	Unresectable extensive primary intra-abdominal disease
	All paraspinal or epidural tumors
Stage IV	Central nervous system and/or bone marrow involvement

21.6.3 Initial Staging with ^{18}F-FDG PET/CT

21.6.3.1 Hodgkin's Disease

Classic HD is strongly ^{18}F-FDG avid in more than 97 % of cases [141, 142] (Fig. 21.7). The ^{18}F-FDG avidity is slightly lower in NLPHL [143]. London et al. found a sensitivity and specificity of 98 and 99.6 % for ^{18}F-FDG PET/CT at initial staging of HD compared with 77 and 98.7 % for conventional anatomical modalities [144]. The high sensitivity and specificity of ^{18}F-FDG PET/CT at initial staging of HD are also confirmed by other authors [145, 146]. ^{18}F-FDG PET/CT has a higher sensitivity than bone marrow biopsy in both adults and children [147–149]. This is probably due to the biopsy site which is usually done from posterior iliac spine. The bone marrow involvement may be patchy or multifocal on ^{18}F-FDG PET/CT [148]. The sensitivity of ^{18}F-FDG PET/CT is lower than chest CT scan for the lung lesions especially if the nodules are less than 5 mm in size [146]. ^{18}F-FDG PET/CT can also be useful for radiotherapy planning. In a study by Girinsky et al., pre-chemotherapy ^{18}F-FDG PET data were essential for correctly implementing the involved-node radiotherapy concept [150]. The other purpose of initial study is to have a baseline for the evaluation of response to therapy. ^{18}F-FDG PET/CT at initial evaluation may be also of interest to guide biopsy [146, 151].

21.6.3.2 Non-Hodgkin's Lymphoma

The risk of bone marrow involvement and presentation at a higher stage (usually stage 3 or 4) is higher in NHL than HD [149, 152]. The aggressive form of NHL is more prevalent in pediatric population than adults; thus, the risk of false-negative ^{18}F-FDG PET study in pediatric NHL is very low [153, 154]. However, since involvement of the brain, kidneys, abdomen, and diffuse bone marrow is relatively common in different types of NHL, the accuracy of ^{18}F-FDG PET/CT may be affected by the physiologic uptake in these organs [155, 156]. Based on the Revised Response Criteria for Malignant Lymphoma (RRCML), ^{18}F-FDG PET is recommended (although is not mandatory yet) at diagnosis, for routine evaluation of

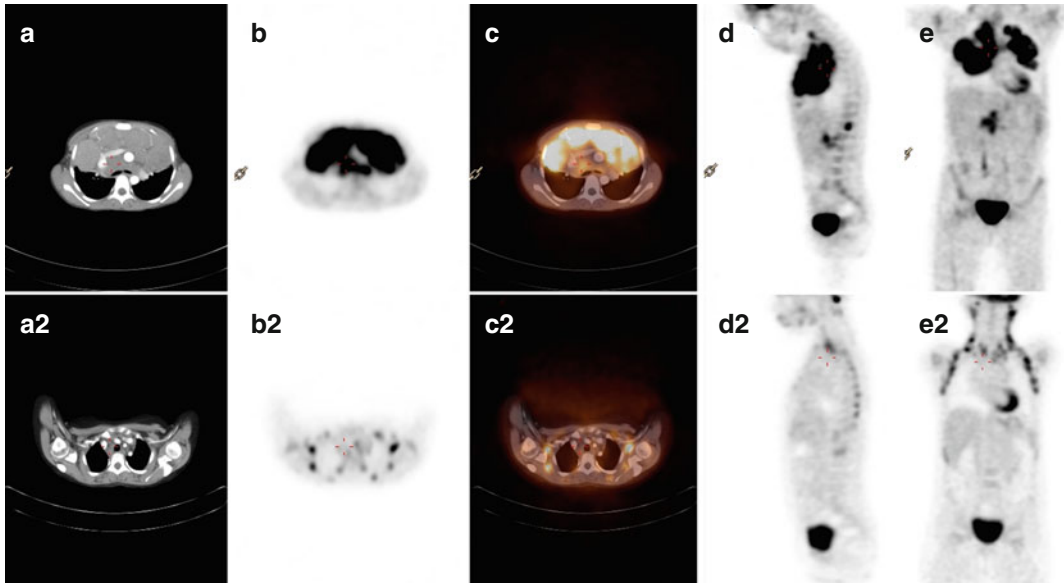

Fig. 21.7 Eight-year-old female with a bulky anterior mediastinal mass diagnosed with Hodgkin's lymphoma. (**a**) Axial CT, (**b**) axial PET, (**c**) axial-fused PET/CT, (**d**) sagittal PET, and (**e**) coronal PET from the 18F-FDG PET/CT performed at initial diagnosis showed a large FDG-avid mass in the anterior mediastinum with multiple foci of increased FDG activity in the supraclavicular regions, spleen, T12, and abdominal lymph nodes (only the anterior mediastinal mass is shown here). The patient is upstaged based on the PET result. After two doses of chemotherapy, (**a2**) axial CT, (**b2**) axial PET, (**c2**) axial-fused PET/CT, (**d2**) sagittal PET, and (**e2**) coronal PET showed marked improvement with minimal residual activity in the mediastinum less than the liver activity suggestive of very good response to therapy. Note is made of multiple foci of FDG activity in the neck and chest corresponding to the hypodense areas on the CT due to brown fat uptake

^{18}F-FDG-avid lymphomas which are curable [157]. There are many reports in which the extranodal involvement is missed by conventional CT scan, particularly in anaplastic large cell lymphomas, DLBC, and Burkitt lymphoma [155, 158, 159]. ^{18}F-FDG PET/CT is also very accurate to detect splenic lesions [145, 160].

21.6.4 Evaluation of Therapy Response with ^{18}F-FDG PET/CT

21.6.4.1 Hodgkin's Disease

^{18}F-FDG PET has an important role in response assessment following chemotherapy in lymphoma even early after a course of therapy (Fig. 21.7). CT scan is a reliable method for staging and restaging of lymphoma. However, the specificity for evaluation of response to therapy is relatively low, especially in patients with bulky disease before treatment [161]. 18F-^{18}F-FDG PET has a high negative predictive value for detection of hypermetabolic tissue after treatment which makes it a reliable method to exclude the presence of any viable residual tumor or recurrence [162].

According to RRCML, although ^{18}F-FDG PET is recommended after completion of chemotherapy, it is not routinely recommended during the therapy [157]. However, the early interim ^{18}F-FDG PET seems to have a prognostic value for therapy response and recurrence [163, 164]. In the EuroNet-PHL-C1 trial (EudraCT 2006-000995-33) that started in 2007, patients will receive the standard treatment including radiotherapy when there is residual viable tissues on the ^{18}F-FDG PET scan after two cycles of chemotherapy [153]. Those with a negative ^{18}F-FDG PET do not receive the radiotherapy at the end of chemotherapy [153, 165]. It should be emphasized that the exact criteria for interpretation of

^{18}F-FDG PET findings after two cycles of chemotherapy have not been fully established, and many factors may affect the interpretation including the time of study, type of tumor, and type of chemotherapy [153]. In a recent study published in New England Journal of Medicine on 602 patients (53.3 % male; median age, 34 years) with Hodgkin's disease, PET scan was performed in 571 patients after third cycles of chemotherapy. The results of PET were negative in 426 of these patients (74.6 %); 420 of those patients were randomly enrolled in two study groups (209 received radiotherapy, and 211 did not receive any further therapy). The results of this study did not show the non-inferiority of the strategy of no further treatment after chemotherapy with regard to progression-free survival based on the PET findings. Moreover, both groups (i.e., with negative PET results after three cycles of chemotherapy), regardless of receiving radiotherapy or not, had a very good prognosis [166].

21.6.4.2 Non-Hodgkin's Lymphoma

Because of limited resolution of PET system and higher prevalence of neoplastic cells in an NHL tumor than HD, a negative PET study at the end of chemotherapy does not necessarily mean there is no viable residual tissue. The interim response to chemotherapy (after two cycle) has probably more prognostic value in this respect [153]. This is important to differentiate those patients who need more intensified chemotherapy versus those who need less therapy to avoid therapy complications [167]. In NHL, a negative interim ^{18}F-FDG PET scan is indicative of a good response and good prognosis [6, 168]. However, this is not confirmed in all types of NHL. In a study by Bakhshi et al., neither interim ^{18}F-FDG PET nor interim CT scan could predict survival [169]. Further studies in different types of NHL in pediatric are needed to clarify the exact role of PET in therapy response of NHL.

21.6.5 Evaluation of Relapse or Recurrence

^{18}F-FDG PET/CT has a sensitivity of 90–100 % to detect residual tissue after therapy. However, the specificity is relatively low with approximately 16–18 % of the cases. False-positive results are due to fibrosis, abdominal wall hernia, inflammation, thymus, and HIV-associated lymphadenopathy [170]. In order to avoid false-positive result due to post-therapeutic inflammation, the study should be done at least 3 weeks after chemotherapy and 2–3 months after radiotherapy. A negative ^{18}F-FDG PET study is a strong indicator of the absence of relapse, while a positive study sometimes warrants further investigation with other imaging modalities or biopsy to confirm the recurrence or relapse [6, 162] (Fig. 21.8).

In summary, ^{18}F-FDG PET is recommended for staging of lymphoma at diagnosis and evaluation of treatment response after completion of therapy. ^{18}F-FDG PET will probably play more roles in the future for the evaluation of therapy response during the treatment (between cycles 1 and 4) and for monitoring the patients, planning the radiation field, and biopsy planning.

21.6.6 Posttransplant Lymphoproliferative Disorder

Posttransplant lymphoproliferative disorder (PTLD) is a relatively uncommon but serious complication of both solid organ and bone marrow transplantation [171, 172]. PTLD comprises of a heterogeneous group of lymphoproliferative diseases, ranging from benign hyperplasia to malignant lymphoma [173]. It is the most common malignancy affecting children after transplantation [174]. The risk of PTLD is higher in children than in adults, probably because of the greater incidence of Epstein–Barr virus (EBV) infection [175, 176]. The overall mortality rate is relatively high [177, 178], but prognosis is likely better in children than in adults [179].

PTLD can be categorized into four major histopathologic types:

(a) Early lymphoid hyperplasia/infectious mononucleosis-type lesions
(b) Polymorphic PTLD

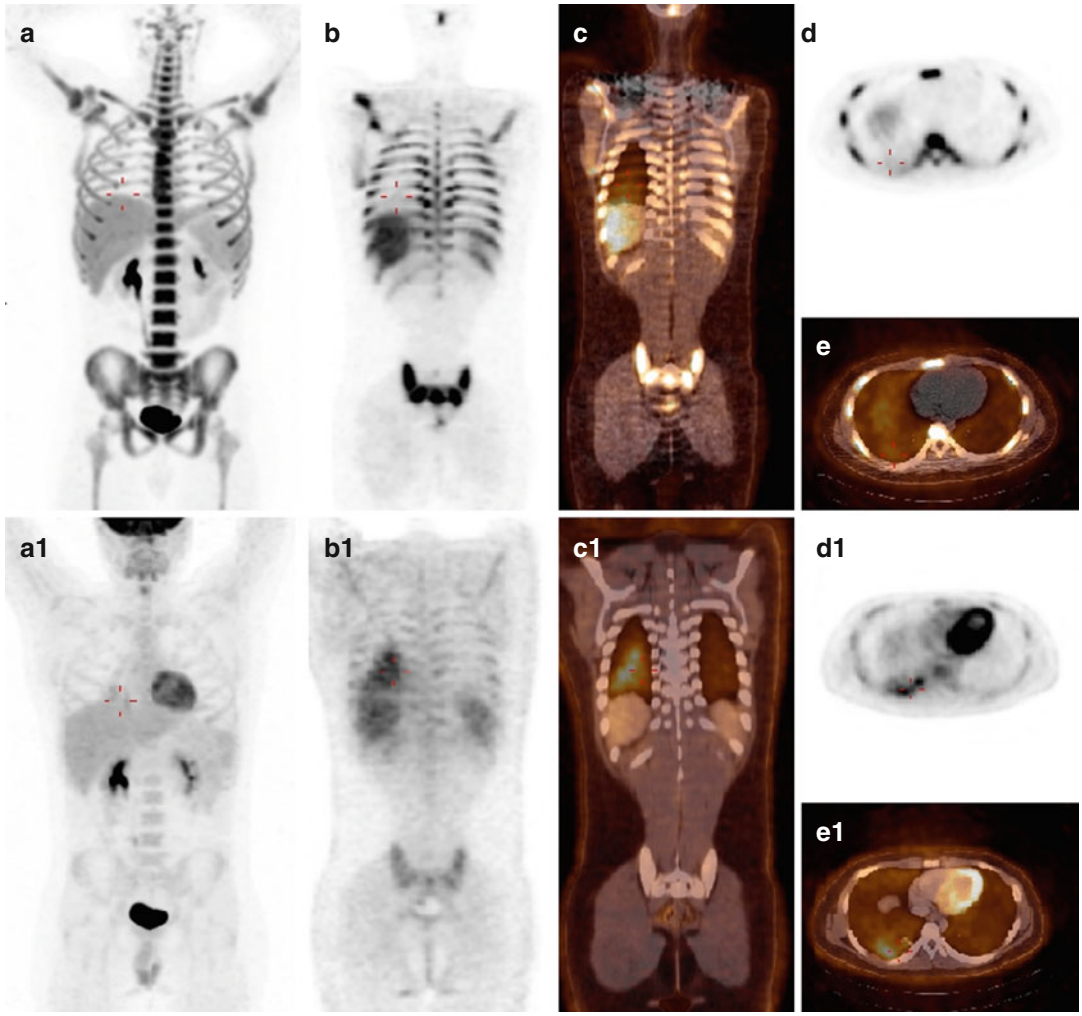

Fig. 21.8 Fifteen-year-old male with Hodgkin's disease after two cycles of chemotherapy. 18F-FDG PET/CT showed mild hilar uptake (not shown here) as well as mild activity in the right basal lung likely due to infection (shown in (**a1**) MIP, (**b1**) coronal PET, (**c1**) coronal-fused PET/CT, (**d1**) axial PET, and (**e1**) axial-fused PET/CT). The right basal lung did not show any increased activity on 18F-FLT (shown in (**a**) MIP, (**b**) coronal PET, (**c**) coronal-fused PET/CT, (**d**) axial PET, and (**e**) axial-fused PET/CT) suggestive of infection rather than tumoral involvement. Note intense activity in the bone marrow on 18F-FLT scan

(c) Monomorphic PTLD, including types 1 and 2, with type 1 including diffuse large B-cell lymphoma (DLBCL), Burkitt lymphoma, and plasma cell myeloma/plasmacytoma-like lesions and type 2 including peripheral and hepatosplenic T-cell lymphomas
(d) Classical Hodgkin-type lymphomas [180]

Although PTLD may occur at any time, it is more common in the first year after transplantation and declines over time [178]. The diagnosis of PTLD is based on histopathology confirmation in following clinical and biochemical suspicion.

Evaluation of the extent of disease is important for the patient treatment management ranging from immunosuppressive therapy during the early phase or surgery on localized lesions to systemic chemotherapy in patients with monomorphous and classical Hodgkin lymphoma-type PTLD. Children with PTLD are usually staged according to the St. Jude staging system of non-Hodgkin's lymphoma (Table 21.4). Computerized

tomography (CT), bone marrow biopsy, and, occasionally, magnetic resonance imaging (MRI) are often used to stage the disease.

Recently ^{18}F-FDG PET/CT showed promising results for staging and response to therapy in PTLD both in adults [181–187] and children [183, 184, 188]. Takehana et al. showed that ^{18}F-FDG PET/CT is useful in the management of patients with PTLD since both nodal and extranodal lesions demonstrated intense ^{18}F-FDG uptake in children [184]. In this study, one of the potential benefits of ^{18}F-FDG PET/CT was the ability to detect occult lesions not visualized on other imaging modalities, particularly extranodal lesion. Other studies showed the usefulness of ^{18}F-FDG PET/CT to evaluate response to therapy in children [183, 188] (Fig. 21.9). Further prospective studies are needed to define the exact role of ^{18}F-FDG PET/CT in staging, response to therapy, and prognosis in pediatric PTLD.

21.7 Leukemia

Leukemias account for 25 % of childhood malignancy and are therefore the most common cause of childhood cancer. Acute lymphoid leukemia (ALL) is the most common form representing approximately 75 % of cases, while acute myeloid leukemia (AML) accounts for most of the remainder. The incidence of ALL peaks at 2–4 years, while AML is most common in neonates or adolescents. There is a Caucasian preponderance.

Ionizing radiation exposure and genetic predisposition have been implicated in the development of ALL. Today ALL has a reasonably good prognosis, particularly in children age 1–10, with overall survival of approximately 80–90 %. Improved treatments are responsible for the dramatic improvements in survival in what was generally a fatal disease in the 1970s. AML carries a more guarded prognosis. Multiple factors have been implicated in the development of AML including genetic predisposition, radiation, medications, and environmental exposures.

The skeleton is commonly involved in leukemia; however imaging is generally not indicated prior to treatment and does not significantly alter management. PET/CT with ^{18}F-FDG usually demonstrates increased skeletal activity due to a combination of tumor infiltration and marrow hyperplasia [189]. ^{18}F-FDG PET has been described to investigate relapse where clinically appropriate or to assess the complications of bone marrow transplant [190]. Caution has been advised in the interpretation of ^{18}F-FDG PET for the workup of ALL in patients receiving high-dose steroid therapy [191], as steroid can alter the biodistribution of ^{18}F-FDG.

21.8 Tumors of the Brain and Central Nervous System

Cancers of the central nervous system make up the most common solid tumors in children and constitute the second most common pediatric malignancy, accounting for 16–20 % of all cancers in children and adolescents. Brain tumors, unfortunately, remain the leading cause of death in children with cancer. Astrocytoms, including the aggressive poorly differentiated astrocytoma, account for 52 % of childhood pediatric malignancies, which primitive neuroectodermal tumors (PNETs) account for 21 % (Fig. 21.10), other tumors of glial origin for 15 %, and ependymomas for 9 % (Table 21.5). Astrocytoma is the most common supratentorial brain tumor in children, many of which can be low grade, and hence there is particular interest and utility in deducing tumor histology from functional imaging. In the third ventricle, hypothalamic gliomas, craniopharyngiomas, and germ cell tumors are most common. In the posterior fossa, medulloblastoma, cerebellar astrocytoma, ependymoma, and brain stem glioma are the most common malignancies. In general, with the major exception of the juvenile pilocytic astrocytoma, the prognosis for central nervous system malignancy in children is poor and is particularly poor in infants with PNET or ependymoma.

Imaging of pediatric brain malignancy is a particularly strong example of the complimentary aspects of all neuroimaging modalities. MRI, with exquisite contrast resolution, is standard in the workup of these patients, as is CT for the

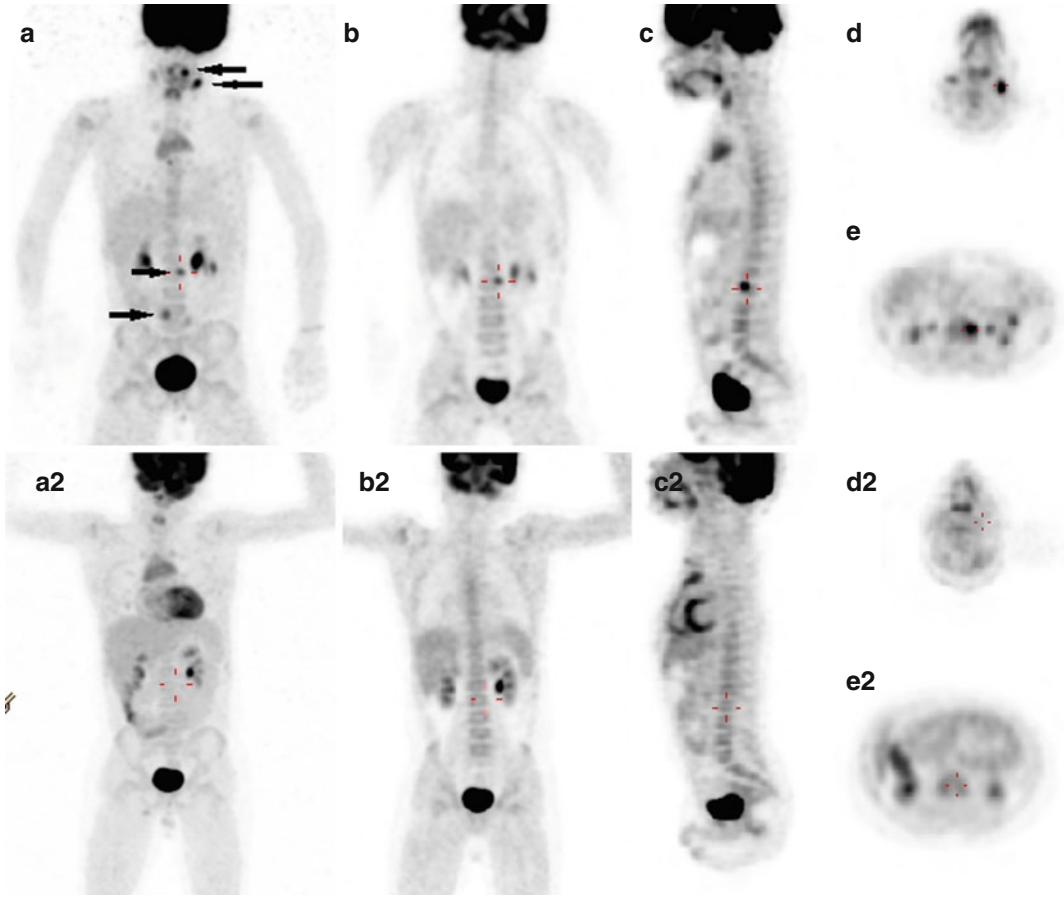

Fig. 21.9 A 7-year-old boy with the diagnosis of PTLD in the tonsils 1 year after lung transplant. 18F-FDG PET/CT was performed to evaluate the extent of the disease. (**a**); MIP image showed multiple foci of increased activity in the tonsil, a neck lymph node, spine, and abdomen (*arrows*). (**b**) Coronal PET, (**c**) sagittal PET, and (**e**) axial PET showed the spine lesion. (**d**) Axial PET showed the neck lymph node. 45 days later after a trial of decreased immune-suppression therapy, the lesions were resolved suggestive of a good response to therapy (see (**a2**) MIP, (**b2**) coronal PET, (**c2**) sagittal PET, (**d2**), axial PET from the neck, and (**e2**) axial PET from the abdomen, after reduced immune-suppression therapy)

evaluation of calcifications and for rapid perioperative assessment. Nuclear medicine continues to find a niche in clinical practice to assess cellular metabolism in these lesions and in adjacent brain parenchyma which often suffers from post-therapeutic change.

PET tracers have been extensively described in the workup of brain and spine malignancy. ^{18}F-FDG PET has been, due to its wide availability, the most widely studied tracer. ^{18}F-FDG activity in a brain tumor has been shown to correlate to histologic grade which in turn influences prognosis [192–194], assesses recurrent tumor [195], as well as determines whether a low-grade tumor is undergoing transition to higher grade [195, 196]. ^{18}F-FDG however suffers to some extent from nonspecificity, as well as uptake in normal brain tissue. Hence an extensive literature has developed in predominantly C11-labeled amino acids in PET imaging [15, 101] as well as choline [197]. C11 methionine is commonly used, and because it is not taken up by brain tissue, it provides excellent target to background ratio and can be used for initial staging/grading, to guide surgery (usually fused to CT or MRI), to assess response to treatment, and to differentiate

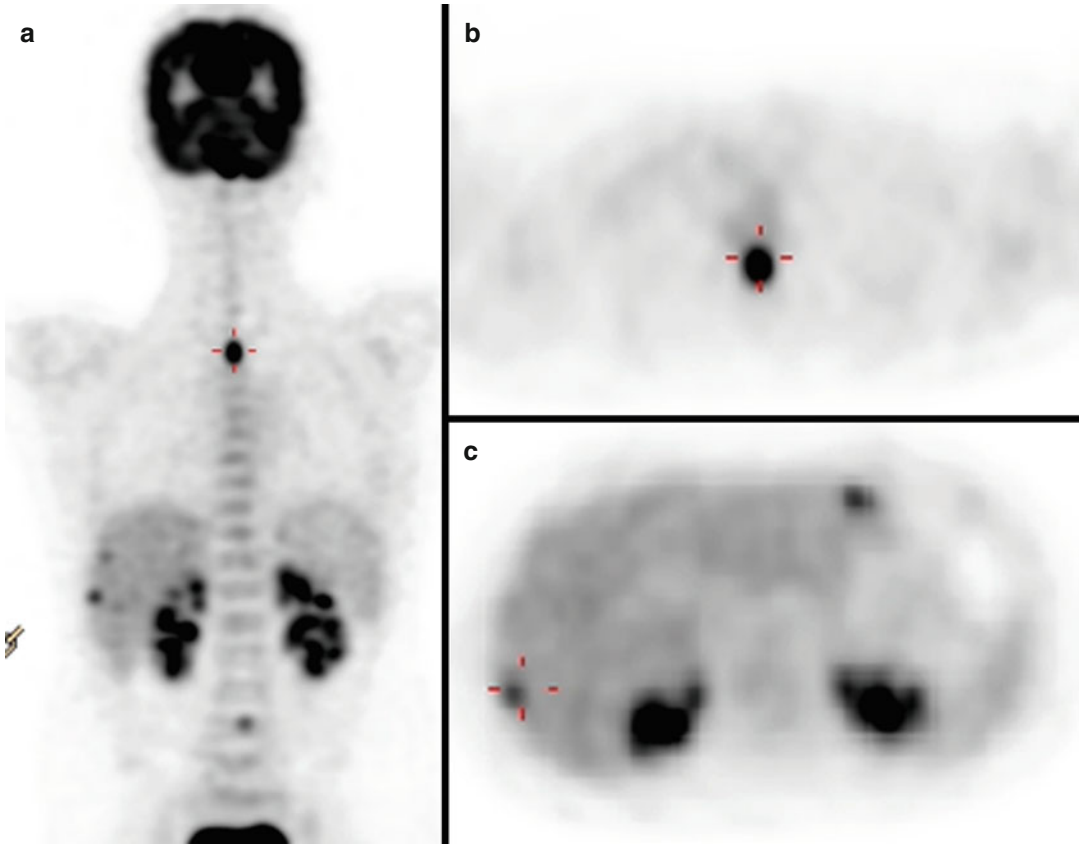

Fig. 21.10 Eleven-year-old boy with PNET. 18F-FDG PET/CT showed multiple FDG-avid lesions in the liver ((**a**) coronal PET and (**c**) axial PET), brain (not shown here), spinal cord ((**a**) coronal PET and (**b**) axial PET), and right iliac crest (nor shown here) suggestive of metastatic disease. Biopsy from the liver lesions confirmed the diagnosis of metastatic PNET

residual/recurrent tumor from scar or other therapeutic changes [198–200].

Since corticosteroids, chemotherapy, and radiation therapy all change cerebral glucose uptake, evaluation of response to chemotherapy with ^{18}F-FDG PET is not very straightforward in pediatric brain tumors [6]. Since ^{18}F-FDG PET and MR spectroscopy have a complementary role in the assessment of brain tumor metabolic activity, the introduction of integrated PET/MR scanners may open new windows for the clinical value of ^{18}F-FDG PET imaging in pediatric brain tumors [6, 201]. Other radiotracers such as ^{18}F-FLT or ^{18}F-DOPA are probably more useful for pediatric brain tumor imaging [82].

21.9 Osseous and Soft Tissue Malignancy

Ewing's sarcoma and osteosarcoma together constitute approximately 6 % of childhood malignancy. The 5-year survival of children with primary bone cancer is improving, with one author citing an increase in survival from 49 % in 1984 to 63 % in 1994. The 5-year survival rate today is generally at or greater than 70 %. The incidence of osteosarcoma is approximately twice that of Ewing's sarcoma, with the incidence of these cancers beginning at age 5 and increasing to peak at approximately age 18.

Table 21.5 WHO histopathologic classification of CNS tumors

Tumor origin	Tumor cell type (examples)
Neuroepithelial tissue	*Astrocytic tumors* (astrocytoma, anaplastic astrocytoma, pilocytic astrocytoma, pleomorphic xanthroastrocytoma, subependymal giant cell astrocytoma)
	Oligodendroglial tumors (oligodendroglioma, anaplastic oligodendroglioma)
	Ependymal tumors (ependymoma, anaplastic ependymoma, myxopapillary ependymoma)
	Neuronal tumors (gangliocytoma, ganglioma, desmoplastic infantile neuroepithelioma, dysembryoplastic neuroepithelial tumor)
	Choroid plexus tumors (choroid plexus papilloma, choroid plexus carcinoma)
	Pineal tumors (pineocytoma, pineoblastoma)
Embryonal origin	*Primary neuroectodermal tumors* (medulloblastoma, neuroblastoma, ependymoblastoma)
	Other embryonal cells (medulloepithelioma, neuroblastoma, ependymoblastoma)
Germ cell	*Germinoma*
	Embryonal carcinoma
	Endodermal sinus tumor
	Choriocarcinoma
	Teratoma
	Mixed germ cell tumors
	Ependymoblastoma
Tumors in the sella turcica	*Pituitary adenoma*
	Craniopharyngioma

21.9.1 Osteosarcoma

The peak incidence of osteosarcoma in children is between 11 and 18 years, with a 5-year survival of between 70 and 80 %. Survival has improved with a combination of neoadjuvant chemotherapy and aggressive surgery. Osteosarcoma is thought to originate in primitive bone-forming mesenchymal stem cells and often arises from the metaphyseal aspect of long bones. The distal femur and proximal tibia/fibula account for half of cases. An association with ionizing radiation, Paget's disease, and genetic susceptibility has been hypothesized. Advances in surgery have improved functional outcome, though surgical resection is still often disfiguring.

Table 21.6 Surgical staging for osteosarcoma

Stage	Description
Stage IA	Low grade, intra-compartmental
Stage IB	Low grade, extra-compartmental
Stage IIA	High grade, intra-compartmental
Stage IIB	High grade, extra-compartmental
Stage III	With metastases

The detection of distant metastases is the most important component of the imaging workup as metastases strongly negatively influence prognosis. Grading of the tumor is the next most important aspect of the workup, including the detection of any extension of tumor outside the anatomic compartment. The majority of osteosarcomas are high grade but remain confined to one anatomic compartment. Children and adolescents commonly present with pain and swelling.

Musculoskeletal plain film is usually followed by MRI for initial diagnosis, which is generally followed by biopsy correlation, bone scan including SPECT of the thorax, and CT of the thorax, abdomen, and pelvis. Plain films often show an aggressive lesion with expansion of the bone and extensive periosteal reaction. MRI of the affected bone is crucial in determining the extent of local spread and the presence of skip lesions. The CT thorax and bone scan SPECT detect metastatic disease to the thorax. Lung and bone are the two most common sites of metastases in osteosarcoma. The surgical staging system of osteosarcoma is provided in Table 21.6.

Prior to the more widespread implementation of ^{18}F-FDG PET, Tc 99m MDP was often the

tracer of choice for total body scan in the osteosarcoma patient. Primary tumor is generally hyperemic on blood flow and pool images and intensely MDP avid on delayed skeletal phase images. Both distant bone and lung metastases are generally MDP avid [202]. Occasionally, bone scan shows changes of associated hypertrophic osteoarthropathy when lung disease is present. Radiotherapy has limited role in the therapy of osteosarcoma for curative intent and is hence reserved for inoperable tumors. Irradiated osteosarcomas can remain MDP avid for months after therapy, and hence other tracers such as ^{18}F-FDG PET or thallium 201 are preferred for this indication. Thallium 201 is an excellent tracer to stage and assess response to treatment in osteosarcoma, as is Tc 99m sestamibi in a more limited literature, where failure of appropriate response tends to indicate more aggressive surgery [203, 204].

^{18}F – FDG PET was described in a prospective study by Volker et al. in 46 patients (Ewing = 23, osteosarcoma = 11, rhabdomyosarcoma = 12) to demonstrate that ^{18}F-FDG PET was as accurate as the combination of all other modalities including MRI and conventional nuclear imaging [205]. Although CT showed better sensitivity to lung metastases (100 % vs. 25 %), PET was superior to all modalities for the detection of metastatic adenopathy (95 % vs 25 %) and osseous lesions (90 % vs. 57 %). A combination of MDP bone scan and ^{18}F-FDG PET was shown to have a higher sensitivity (100 %) for the detection of bone metastases compared to ^{18}F-FDG PET (92 %) or bone scan (74 %) alone [206]. ^{18}F-FDG PET may be of less value than conventional tracers in predicting response to chemotherapy, as a study by Huang et al. demonstrated a tumor necrosis rate of 22 % by ^{18}F-FDG PET compared to 55 % necrosis on pathology in the same series of ten patients [207]. Thus, though some authors have had better success [208, 209], ^{18}F-FDG PET may underestimate response to therapy and should be used with caution for this indication in the osteosarcoma patient.

Fluorine-18-labeled sodium fluoride (^{18}F-NaF) has also been used in pediatrics in different clinical indications. The biodistribution of ^{18}F-NaF is similar to that of ^{99m}Tc-MDP [67]. However, there are some advantages with ^{18}F-NaF PET compared with the conventional bone scan. First, the extraction of the ^{18}F-NaF by bone is faster than ^{99m}Tc-MDP due to its lower protein binding. Thus, it allows for earlier imaging. Secondly, the extraction of the radiotracer is greater than MDP, so the target to background ratio is higher. Finally, the resolution of PET system is better than that of conventional gamma cameras. All these factors allow for obtaining higher-quality images with ^{18}F-NaF PET. Although there are many reports showing promising results with ^{18}F-NaF PET/CT to detect bone metastases in different tumors in adults, to our knowledge, there is no report focusing on using ^{18}F-NaF in detecting bone metastases in children. However, it seems that it can be very useful in children especially for tumors with lesser uptake on bone scan such as LCH. Further studies are needed to evaluate the exact role of ^{18}F-NaF PET/CT in pediatric oncology. The radiation absorbed dose is similar or only slightly more than that of ^{99m}Tc-MDP bone scan [67].

21.9.2 Ewing's Sarcoma

Ewing's sarcoma is the second most common bone tumor in children, representing 3 % of childhood malignancies, and represents a family of small round cell tumors. Ewing's sarcoma can occur in intraosseous or extraosseous form or as a peripheral primitive neuroectodermal tumor, neuroepithelioma, or Askin tumor. Ewing's most likely originates from neural crest cells and can arise in either the appendicular or axial skeleton. There is a predilection to Caucasians.

The overall 5-year survival for Ewing's is 70 %, with younger children demonstrating better overall survival than older children or adults. Approximately 25 % of patients have distant metastases at the time of treatment. Prognosis is a function of resectability of the primary (i.e., appendicular versus axial skeletal involvement), presence of distant metastases, and response to chemotherapy. The lymph nodes, bone, and lungs are the most common sites of distant metastases, though any organ can be affected.

The diagnosis is usually made by tissue biopsy after a lesion is worked up by X-ray and MRI. MRI is warranted to assess the entire bone occupied by tumor for skip lesions. Bone scan demonstrates a more homogenous pattern of uptake than the generally more heterogenous uptake seen in osteosarcoma. The distribution of tumor is generally more diaphyseal or metadiaphyseal compared to osteosarcoma which is usually situated at the metaphysis. Diagnostic chest CT is the modality of choice for the assessment of lung metastases [205].

Bone metastases are ultimately detected in 33–45 % of patients who were free of metastatic disease at presentation. Thus serial ^{18}F-FDG PET scans or bone scans are usually performed in the first 2 years after diagnosis to detect any occult disease. Erlemann et al. demonstrated that assessment of the primary tumor on MRI provided a more accurate assessment of therapeutic response than did bone scan (85 % versus 50 %) and thus if bone scan does not demonstrate improvement with therapy, MRI is indicated for further assessment [210]. Definite decrease in MDP uptake at the tumor site does indicate response.

Although as in osteosarcoma, ^{18}F-FDG PET has value equal or exceeding conventional tracers for the initial staging of Ewing's sarcoma, for Ewing in particular ^{18}F-FDG PET does not have value for the assessment of response to treatment [211]. Both responders and nonresponders can have decreased ^{18}F-FDG activity at tumor sites. As in osteosarcoma, CT thorax has greater sensitivity than ^{18}F-FDG PET for the detection of pulmonary metastases, and so diagnostic CT thorax is needed in addition to PET/CT if the CT component of the PET is not of diagnostic quality [205].

21.9.3 Rhabdomyosarcoma

Rhabdomyosarcoma (RMS) is an aggressive tumor demonstrating bimodal peaks of incidence between the ages of 2–5 years and 15–19 years (Table 21.7). The survival rate has improved from 20 % in the 1960s to 70 % today, mainly due to accurate imaging of the local disease extension and effective surgical resection. There is a role for radiotherapy in the treatment of local disease. Distant metastases are associated with poor prognosis. Other factors associated with poor prognosis include unfavorable sites of primary disease such as the meninges, bladder/prostate, retroperitoneum, extremities, and abdomen, as well as alveolar type, poorly differentiated histology, large tumor size (i.e., > 5 cm), nodal involvement, elderly age, and local/nodal or bone mets. RMS accounts for 4–8 % of malignancy in children less than 15 years old. The etiology of RMS is poorly understood with some association documented between incidence and other genetic diseases including neurofibromatosis 1, Gorlin syndrome, retinoblastoma syndrome, Costello syndrome, Rubinstein–Taybi syndrome, and Beckwith–Wiedemann. Maternal substance abuse has also been linked to the development of RMS.

^{18}F – FDG PET has been described for the workup of RMS. ^{18}F-FDG uptake widely varies

Table 21.7 TNM Staging of rhabdomyosarcoma

Stage	Description
Stage I	T1 or T2 (a or b), N0/1/x and M0 and in favorable site: head and neck (excluding parameningeal), orbit, genitourinary (non-bladder/non-prostate), biliary tract
Satge II	T1 or T2 a (not b), N0 or Nx (not N1) and M0; site: bladder and/or prostate, extremity, cranial parameningeal, other areas including trunk, retroperitoneum, etc.
Satge III	T1 or T2 a, N1, M0 in bladder and/or prostate or T1 or T2b, N0 or N1 or Nx, M0 in extremity, cranial parameningeal, and others including trunk, retroperitoneum, etc., except the biliary tract
Stage IV	M1 (irrespective of T and N and the site of tumor)

T1 = Confined to anatomic site of origin ((a) if diameter is ≤ 5 cm; (b) if diameter is > 5 cm)
T2 = Extension and/or invasion to surrounding tissue ((a) if diameter is ≤ 5 cm; (b) if diameter is > 5 cm)
N0 = Regional nodes not clinically involved
N1 = Regional nodes clinically involved by tumor
Nx = Clinical status of regional nodes unknown (especially sites where lymph node evaluation is not possible)
M0 = No distant metastasis
M1 = With distant metastasis

in RMS [212]. Increased ^{18}F-FDG activity at the site of primary tumor is associated with poor differentiation and hence overall more aggressive tumor and worse prognosis [213, 214]. ^{18}F-FDG also shows excellent sensitivity to the detection of local disease and distance metastases, including metastatic adenopathy and bone metastases. Several authors have shown ^{18}F-FDG PET to be superior in terms of the accurate detection of distance metastases to a combination of conventional modalities including CT, MRI, and bone scintigraphy [94, 215]. The exception is in the detection of pulmonary metastases, to which ^{18}F-FDG PET can be insensitive. Therefore, diagnostic CT is indicated in the RMS patient. ^{18}F-FDG PET is also capable of accurately detecting recurrent disease or relapse where there has been prior treatment.

21.10 Nephroblastoma (Wilms' Tumor)

The Wilms' tumor is the most common form of pediatric renal malignancy, accounting for 95 % of renal cancers in children and 6 % of all childhood cancer (Table 21.8). The peak age of incidence for Wilms' tumor is 3–4 years, and the cancer is generally felt to most commonly affect children less than years old. Due to a slow indolent growth pattern, earlier detection, and aggressive surgical management, the 5-year survival rate of children with Wilms' tumor is approximately 90 %. The etiology of Wilms' tumor is unknown and likely sporadic; however a minority of cases (~5 %) are associated with genetic defects including Beckwith–Wiedemann, Denys–Drash, and Perlman syndromes. When metastases are present, the lung and liver are most commonly involved.

Table 21.8 Staging system used for Wilms' Tumor

Stage	Description
Stage I	Tumor limited to kidney (completely excised)
Stage II	Tumor extends beyond the kidney (but is completely removed)
Stage III	More than one of the following criteria must be met:
	1. Unresectable primary tumor
	2. Lymph node involvement
	3. Positive surgical margins
	4. Tumor spillage involving peritoneal surfaces either before or during surgery or transected tumor thrombus
Stage IV	Hematogenous metastases
Stage V	Bilateral renal involvement at initial diagnosis

The workup of Wilms' tumor at time of presentation usually includes an initial abdominal ultrasound followed by CT scan with contrast. Patients often present with an asymptomatic abdominal mass; however it can also present with abdominal pain, hypertension, fever, hematuria, anemia, and weight loss. The extent of local invasion and venous extension is generally determined by conventional imaging modalities such as ultrasound and CT. ^{18}F-FDG PET, because of renal excretion of ^{18}F-FDG and consequent poor target to background, can be less useful than conventional imaging for the assessment of the primary renal mass. ^{18}F-FDG PET/CT however may have some role in the assessment of liver and lung metastases or other distant spread [216]. One author has used ^{18}F-FDG PET to assess response to therapy [217].

21.11 Hepatoblastoma

The hepatoblastoma and hepatoma are the two most common hepatic malignancies in children, with hepatoblastoma occupying the majority (~2/3) of cases. Hepatoma occupies most of the remaining cases. Hepatic malignancy is uncommon in children, representing approximately 1 % of childhood cancer.

Hepatoblastoma is most common in children under the age of 5 years. The pathophysiology of hepatoblastoma is not well characterized, likely in part due to the rarity of the tumor. With a combination of aggressive surgery, chemotherapy, and sometimes radiotherapy, the 5-year survival rate for hepatoblastoma is 60 %.

Hepatocellular carcinoma generally affects children over the age of 10, and due to a

combination of local aggressiveness and metastatic spread prior to detection, it is associated with a more pessimistic prognosis.

The liver normally demonstrates mild diffuse ^{18}F-FDG activity. Fatty infiltration, which is not uncommon in children, can demonstrate ^{18}F-FDG accumulation which can be confused with malignancy. Conventional imaging modalities such as ultrasound, CT, and MRI are generally used more extensively than PET for the workup of hepatic tumors. Where ^{18}F-FDG PET has been utilized, increased ^{18}F-FDG uptake is associated with more aggressive tumor grade and poor prognosis [218, 219]. There has been meaningful progress in the combination of ^{18}F-FDG uptake and alpha fetoprotein to detect recurrence of tumor after therapy [218]. A decrease in ^{18}F-FDG uptake in a tumor post-therapy is associated with response [219]. In addition, if alpha fetoprotein is negative, ^{18}F-FDG PET can be used for a systemic screening for poorly differentiated distant metastases in a manner analogous to thyroid malignancy [219].

The PET literature in pediatric hepatic malignancy is limited, partially due to the rarity of the tumor, and consists primarily of small case series. There would be significant benefit to the future examination of larger series of cases.

21.12 Thyroid Malignancy

Thyroid cancer is the most common type of endocrine cancer accounting for 1–1.5 % of all pediatric malignancies. Thyroid cancer is very rare in early childhood; the peak age is in the 15–19-year-old group. The majority of thyroid cancers are of differentiated type, mainly papillary (85 %) and to a lesser extent follicular cancer (10 %). The exact cause is unknown; however, there are many risk factors that may increase the risk of thyroid cancers, including ionizing radiation, family history of thyroid cancer, female gender, and sex hormones. The incidence is higher in females; however, the prognosis is slightly worse in males.

131-I has a major role in the management of the thyroid cancer for both diagnosis and ablation therapy. The role of PET in thyroid cancer is limited to the cases of negative iodine scan and positive serum thyroglobulin level. The spectrum of well differentiated to undifferentiated thyroid cancer corresponds to the spectrum of iodine versus ^{18}F-FDG avidity, respectively [220]. That is, while well-differentiated thyroid cancers are generally hot on iodine scintigraphy, more clinically aggressive undifferentiated tumors tend to be hot on ^{18}F-FDG PET. Thus, ^{18}F-FDG PET is generally the imaging tool of choice for the workup of a patient with elevated or rising thyroglobulin where iodine imaging has been negative [221, 222]. In this clinical scenario, it has been the author's experience that metastatic adenopathy can demonstrate ^{18}F-FDG avidity, and hence morphologic features on corresponding CT are important to assess along with activity.

The incidence of medullary thyroid cancer is very rare in children (about 2 % of thyroid cancers). The information about the diagnosis and treatment of medullary thyroid cancer in children is very limited and is usually extrapolated from the adult data. Laboratory examination (serum calcitonin level, CEA measurement, etc.), ultrasound, CT scan, 99mTc(pentavalent)-DMSA study, ^{18}F-FDG PET/CT, and ^{18}F-DOPA PET/CT have been used to detect and follow up lesions [223, 224].

Conclusion

Combined ^{18}F-FDG PET/CT is being used more frequently in the evaluation of various malignancies in pediatric patients including lymphomas, soft tissue tumors, and bone sarcomas. PET/CT can provide valuable information that is not apparent on anatomical imaging for staging and monitoring response to therapy. The growing evidence supports the continued investigation of PET and PET/CT imaging in the management and surveillance of pediatric malignancies.

Using ^{18}F-FDG PET/CT in children requires an awareness of the technical and logistical issues unique to children such as sedation or anesthesia. Adequate preparation of patients

and families is essential. A thorough knowledge and understanding of the normal distribution of ^{18}F-FDG uptake in children, normal variants of pediatric ^{18}F-FDG PET/CT, and artifacts are necessary for accurate image interpretation of pediatric PET/CT imaging that differs from those of adults.

With the introduction of new imaging techniques such as PET/MR or diffusion MRI, it is expected to have an emerging role in pediatric oncology imaging with lower radiation burden compared to PET/CT. However, the exact role and value are not well established yet and further investigation is needed. Newer radiotracers such as ^{68}Ga-DOTA, ^{18}F-DOPA, ^{18}F-FAZA, and ^{18}F-FLT may be used in specific pediatric tumors. ^{18}F- NaF can be used for skeletal imaging in malignant disease. Tumor receptor imaging has the potential to improve tumor detection and characterization.

References

1. Davidoff AM. Pediatric oncology. Semin Pediatr Surg. 2010;19(3):225–33.
2. Siegel R, Naishadham D, Jemal A. Cancer statistics, 2012. CA Cancer J Clin. 2012;62(1):10–29.
3. Steliarova-Foucher E, et al. International classification of childhood cancer, third edition. Cancer. 2005;103(7):1457–67.
4. Steliarova-Foucher E, et al. Trends in childhood cancer incidence in Europe, 1970–99. Lancet. 2005;365(9477):2088.
5. SEER NCI. The Survival, Epidemiology, and End Result Program: SEER stats fact sheet: thyroid cancer. National Cancer Institute. 2014. http://seer.cancer.gov/statfacts/html/thyro.html.
6. Uslu L, et al. Value of 18F-FDG PET and PET/CT for evaluation of pediatric malignancies. J Nucl Med. 2015;56(2):274–86.
7. Gulyas B, Halldin C. New PET radiopharmaceuticals beyond FDG for brain tumor imaging. Q J Nucl Med Mol Imaging. 2012;56(2):173–90.
8. Persson M, et al. 68Ga-labeling and in vivo evaluation of a uPAR binding DOTA- and NODAGA-conjugated peptide for PET imaging of invasive cancers. Nucl Med Biol. 2012;39(4):560–9.
9. Fernandes E, et al. Positron emitting tracers in preclinical drug development. Curr Radiopharm. 2012;5(2):90–8.
10. Prezzi D, Khan A, Goh V. Perfusion CT imaging of treatment response in oncology. Eur J Radiol. 2015;84:2380–5.
11. Coursey CA, et al. Dual-energy multidetector CT: how does it work, what can it tell us, and when can we use it in abdominopelvic imaging? Radiographics. 2010;30(4):1037–55.
12. Lee YH, et al. Spectral parametric segmentation of contrast-enhanced dual-energy CT to detect bone metastasis: feasibility sensitivity study using whole-body bone scintigraphy. Acta Radiol. 2015;56(4):458–64.
13. Brady SL, Shulkin BL. Ultralow dose computed tomography attenuation correction for pediatric PET CT using adaptive statistical iterative reconstruction. Med Phys. 2015;42(2):558–66.
14. Schafer JF, et al. Simultaneous whole-body PET/MR imaging in comparison to PET/CT in pediatric oncology: initial results. Radiology. 2014;273(1):220–31.
15. Dunkl V, et al. The usefulness of dynamic O-(2-18F-fluoroethyl)-L-tyrosine PET in the clinical evaluation of brain tumors in children and adolescents. J Nucl Med. 2015;56(1):88–92.
16. Misch M, et al. (18)F-FET-PET guided surgical biopsy and resection in children and adolescence with brain tumors. Childs Nerv Syst. 2015;31(2):261–7.
17. Fraioli F, et al. 18F-fluoroethylcholine (18F-Cho) PET/MRI functional parameters in pediatric astrocytic brain tumors. Clin Nucl Med. 2015;40(1):e40–5.
18. Kurihara Y, et al. MRI of pulmonary nodules. AJR Am J Roentgenol. 2014;202(3):W210–6.
19. Loeffelbein DJ, et al. PET-MRI fusion in head-and-neck oncology: current status and implications for hybrid PET/MRI. J Oral Maxillofac Surg. 2012;70(2):473–83.
20. Buckwalter KA, Lin C, Ford JM. Managing postoperative artifacts on computed tomography and magnetic resonance imaging. Semin Musculoskelet Radiol. 2011;15(4):309–19.
21. Hendee WR, O'Connor MK. Radiation risks of medical imaging: separating fact from fantasy. Radiology. 2012;264(2):312–21.
22. Dobyns BM, et al. Malignant and benign neoplasms of the thyroid in patients treated for hyperthyroidism: a report of the cooperative thyrotoxicosis therapy follow-up study. J Clin Endocrinol Metab. 1974;38(6):976–98.
23. Ron E, et al. Cancer mortality following treatment for adult hyperthyroidism. Cooperative Thyrotoxicosis Therapy Follow-up Study Group. JAMA. 1998;280(4):347–55.
24. Fahey FH, Treves ST, Adelstein SJ. Minimizing and communicating radiation risk in pediatric nuclear medicine. J Nucl Med. 2011;52(8):1240–51.
25. Preston DL, et al. Studies of mortality of atomic bomb survivors. Report 13: solid cancer and noncancer disease mortality: 1950–1997. Radiat Res. 2003;160(4):381–407.
26. Turner HC, et al. Effect of dose rate on residual gamma-H2AX levels and frequency of micronuclei in X-irradiated mouse lymphocytes. Radiat Res. 2015;183(3):315–24.

27. Pouliliou S, Koukourakis MI. Gamma histone 2AX (gamma-H2AX) as a predictive tool in radiation oncology. Biomarkers. 2014;19(3):167–80.
28. Huda W. Radiation risks: what is to be done? AJR Am J Roentgenol. 2015;204(1):124–7.
29. Ng AK, et al. Secondary malignancies across the age spectrum. Semin Radiat Oncol. 2010;20(1):67–78.
30. Fridlich R, et al. BRCA1 and BRCA2 protect against oxidative DNA damage converted into double-strand breaks during DNA replication. DNA Repair (Amst). 2015;30:11–20.
31. Drooger JC, et al. Diagnostic and therapeutic ionizing radiation and the risk of a first and second primary breast cancer, with special attention for BRCA1 and BRCA2 mutation carriers: a critical review of the literature. Cancer Treat Rev. 2015; 41(2):187–96.
32. Piechowiak EI, et al. Intravenous iodinated contrast agents amplify DNA radiation damage at CT. Radiology. 2015;275:692–7. doi:10.1148/radiol.14132478.
33. Lacaille H, et al. Comparison of the deleterious effects of binge drinking-like alcohol exposure in adolescent and adult mice. J Neurochem. 2015; 132(6):629–41.
34. Heydenreich J, et al. Reliability of a fully automated interpretation of gamma -H2AX foci in lymphocytes of moderately trained subjects under resting conditions. J Nutr Metab. 2014;2014:478324.
35. Gelfand MJ. Dose reduction in pediatric hybrid and planar imaging. Q J Nucl Med Mol Imaging. 2010;54(4):379–88.
36. Accorsi R, Karp JS, Surti S. Improved dose regimen in pediatric PET. J Nucl Med. 2010;51(2):293–300.
37. Lassmann M, et al. The new EANM paediatric dosage card. Eur J Nucl Med Mol Imaging. 2007;34(5):796–8.
38. Gelfand MJ, et al. Pediatric radiopharmaceutical administered doses: 2010 North American consensus guidelines. J Nucl Med. 2011;52(2):318–22.
39. American Academy of P, et al. Guidelines for monitoring and management of pediatric patients during and after sedation for diagnostic and therapeutic procedures: an update. Pediatrics. 2006;118(6): 2587–602.
40. Arlachov Y, Ganatra RH. Sedation/anaesthesia in paediatric radiology. Br J Radiol. 2012;85(1019): e1018–31.
41. Delbeke D, et al. Procedure guideline for tumor imaging with 18F-FDG PET/CT 1.0. J Nucl Med. 2006;47(5):885–95.
42. Shen G, et al. Potential performance of dual-time-point 18F-FDG PET/CT compared with single-time-point imaging for differential diagnosis of metastatic lymph nodes: a meta-analysis. Nucl Med Commun. 2014;35(10):1003–10.
43. Shen G, et al. Diagnostic value of dual time-point 18 F-FDG PET/CT versus single time-point imaging for detection of mediastinal nodal metastasis in non-small cell lung cancer patients: a meta-analysis. Acta Radiol. 2015;56:681–7.
44. Costantini DL, et al. Dual-time-point FDG PET/CT for the evaluation of pediatric tumors. AJR Am J Roentgenol. 2013;200(2):408–13.
45. Zukotynski KA, et al. Constant ambient temperature of 24 degrees C significantly reduces FDG uptake by brown adipose tissue in children scanned during the winter. Eur J Nucl Med Mol Imaging. 2009;36(4): 602–6.
46. Shammas A, Lim R, Charron M. Pediatric FDG PET/CT: physiologic uptake, normal variants, and benign conditions. Radiographics. 2009;29(5): 1467–86.
47. Keyes Jr JW. SUV: standard uptake or silly useless value? J Nucl Med. 1995;36(10):1836–9.
48. Ghanem MA, Kazim NA, Elgazzar AH. Impact of obesity on nuclear medicine imaging. J Nucl Med Technol. 2011;39(1):40–50.
49. Krak NC, et al. Effects of ROI definition and reconstruction method on quantitative outcome and applicability in a response monitoring trial. Eur J Nucl Med Mol Imaging. 2005;32(3):294–301.
50. Boellaard R, et al. Effects of noise, image resolution, and ROI definition on the accuracy of standard uptake values: a simulation study. J Nucl Med. 2004;45(9):1519–27.
51. Bemben MG, et al. Age-related variability in body composition methods for assessment of percent fat and fat-free mass in men aged 20–74 years. Age Ageing. 1998;27(2):147–53.
52. Nakahara T, et al. FDG uptake in the morphologically normal thymus: comparison of FDG positron emission tomography and CT. Br J Radiol. 2001;74(885):821–4.
53. Francis IR, et al. The thymus: reexamination of age-related changes in size and shape. AJR Am J Roentgenol. 1985;145(2):249–54.
54. Brink I, et al. Increased metabolic activity in the thymus gland studied with 18F-FDG PET: age dependency and frequency after chemotherapy. J Nucl Med. 2001;42(4):591–5.
55. Ferdinand B, Gupta P, Kramer EL. Spectrum of thymic uptake at 18F-FDG PET. Radiographics. 2004;24(6):1611–6.
56. Sasaki M, et al. Differential diagnosis of thymic tumors using a combination of 11C-methionine PET and FDG PET. J Nucl Med. 1999;40(10): 1595–601.
57. Heusner TA, et al. Incidental head and neck (18) F-FDG uptake on PET/CT without corresponding morphological lesion: early predictor of cancer development? Eur J Nucl Med Mol Imaging. 2009;36(9):1397–406.
58. Elstrom RL, et al. Enhanced marrow [18F]fluorodeoxyglucose uptake related to myeloid hyperplasia in Hodgkin's lymphoma can simulate lymphoma involvement in marrow. Clin Lymphoma. 2004;5(1):62–4.
59. Knopp MV, et al. Bone marrow uptake of fluorine-18-fluorodeoxyglucose following treatment with hematopoietic growth factors: initial evaluation. Nucl Med Biol. 1996;23(6):845–9.

60. Trout AT, et al. Optimizing the interval between G-CSF therapy and F-18 FDG PET imaging in children and young adults receiving chemotherapy for sarcoma. Pediatr Radiol. 2015;45:1001–6.
61. Aflalo-Hazan V, et al. Increased FDG uptake by bone marrow in major beta-thalassemia. Clin Nucl Med. 2005;30(11):754–5.
62. Plantade A, et al. Diffusely increased F-18 FDG uptake in bone marrow in a patient with acute anemia and recent erythropoietin therapy. Clin Nucl Med. 2003;28(9):771–2.
63. Hong TS, et al. Brown adipose tissue 18F-FDG uptake in pediatric PET/CT imaging. Pediatr Radiol. 2011;41(6):759–68.
64. Lin EC, Alavi A. PET and PET/CT: a clinical guide. 2nd ed. New York: Thieme Medical Publishers Inc.; 2009.
65. Bhargava P, Hanif M, Nash C. Whole-body F-18 sodium fluoride PET-CT in a patient with renal cell carcinoma. Clin Nucl Med. 2008;33(12):894–5.
66. Even-Sapir E, et al. Assessment of malignant skeletal disease: initial experience with 18F-fluoride PET/CT and comparison between 18F-fluoride PET and 18F-fluoride PET/CT. J Nucl Med. 2004;45(2):272–8.
67. Segall G, et al. SNM practice guideline for sodium 18F-fluoride PET/CT bone scans 1.0. J Nucl Med. 2010;51(11):1813–20.
68. Bading JR, Shields AF. Imaging of cell proliferation: status and prospects. J Nucl Med. 2008;49 Suppl 2:64S–80.
69. Buck AK, et al. Clinical relevance of imaging proliferative activity in lung nodules. Eur J Nucl Med Mol Imaging. 2005;32(5):525–33.
70. Everitt S, et al. Imaging cellular proliferation during chemo-radiotherapy: a pilot study of serial 18F-FLT positron emission tomography/computed tomography imaging for non-small-cell lung cancer. Int J Radiat Oncol Biol Phys. 2009;75(4):1098–104.
71. Yamamoto Y, et al. Correlation of 18F-FLT and 18F-FDG uptake on PET with Ki-67 immunohistochemistry in non-small cell lung cancer. Eur J Nucl Med Mol Imaging. 2007;34(10):1610–6.
72. Yap CS, et al. Evaluation of thoracic tumors with 18F-fluorothymidine and 18F-fluorodeoxyglucose-positron emission tomography. Chest. 2006;129(2):393–401.
73. Kameyama R, et al. Detection of gastric cancer using 18F-FLT PET: comparison with 18F-FDG PET. Eur J Nucl Med Mol Imaging. 2009;36(3):382–8.
74. Yamamoto Y, et al. Detection of colorectal cancer using 18F-FLT PET: comparison with 18F-FDG PET. Nucl Med Commun. 2009;30:841–5.
75. Cobben DC, et al. 3′-18F-fluoro-3′-deoxy-L-thymidine: a new tracer for staging metastatic melanoma? J Nucl Med. 2003;44(12):1927–32.
76. Buck AK, et al. Molecular imaging of proliferation in malignant lymphoma. Cancer Res. 2006;66(22):11055–61.
77. Herrmann K, et al. Early response assessment using 3′-deoxy-3′-[18F]fluorothymidine-positron emission tomography in high-grade non-Hodgkin's lymphoma. Clin Cancer Res. 2007;13(12):3552–8.
78. Kenny L, et al. Imaging early changes in proliferation at 1 week post chemotherapy: a pilot study in breast cancer patients with 3′-deoxy-3′-[18F]fluorothymidine positron emission tomography. Eur J Nucl Med Mol Imaging. 2007;34(9):1339–47.
79. Pio BS, et al. Usefulness of 3′-[F-18]fluoro-3′-deoxythymidine with positron emission tomography in predicting breast cancer response to therapy. Mol Imaging Biol. 2006;8(1):36–42.
80. Buck AK, et al. Imaging bone and soft tissue tumors with the proliferation marker [18F]fluorodeoxythymidine. Clin Cancer Res. 2008;14(10):2970–7.
81. Choi SJ, et al. [18F]3′-deoxy-3′-fluorothymidine PET for the diagnosis and grading of brain tumors. Eur J Nucl Med Mol Imaging. 2005;32(6):653–9.
82. Gilles R, et al. (18)F-fluoro-L-thymidine-PET for the evaluation of primary brain tumours in children: a report of three cases. Nucl Med Commun. 2010;31(6):482–7.
83. Hatakeyama T, et al. 11C-methionine (MET) and 18F-fluorothymidine (FLT) PET in patients with newly diagnosed glioma. Eur J Nucl Med Mol Imaging. 2008;35(11):2009–17.
84. Saga T, et al. Evaluation of primary brain tumors with FLT-PET: usefulness and limitations. Clin Nucl Med. 2006;31(12):774–80.
85. Tripathi M, et al. Comparative evaluation of F-18 FDOPA, F-18 FDG, and F-18 FLT-PET/CT for metabolic imaging of low grade gliomas. Clin Nucl Med. 2009;34(12):878–83.
86. Shields AF. Positron emission tomography measurement of tumor metabolism and growth: its expanding role in oncology. Mol Imaging Biol. 2006;8(3):141–50.
87. Shields AF, et al. Imaging proliferation in vivo with FLT and positron emission tomography. Nat Med. 1998;4(11):1334–6.
88. Vaupel P, Mayer A. Hypoxia in cancer: significance and impact on clinical outcome. Cancer Metastasis Rev. 2007;26(2):225–39.
89. Harrison LB, et al. Impact of tumor hypoxia and anemia on radiation therapy outcomes. Oncologist. 2002;7(6):492–508.
90. Molls M, et al. Relevance of oxygen in radiation oncology. Mechanisms of action, correlation to low hemoglobin levels. Strahlenther Onkol. 1998;174 Suppl 4:13–6.
91. Hockel M, et al. Association between tumor hypoxia and malignant progression in advanced cancer of the uterine cervix. Cancer Res. 1996;56(19):4509–15.
92. Hockel M, et al. Hypoxia and radiation response in human tumors. Semin Radiat Oncol. 1996;6(1):3–9.
93. Bottaro DP, Liotta LA. Cancer: out of air is not out of action. Nature. 2003;423(6940):593–5.
94. Dorie MJ, Brown JM. Modification of the antitumor activity of chemotherapeutic drugs by the hypoxic

cytotoxic agent tirapazamine. Cancer Chemother Pharmacol. 1997;39(4):361–6.
95. Papadopoulou MV, Bloomer WD. NLCQ-1 (NSC 709257): exploiting hypoxia with a weak DNA-intercalating bioreductive drug. Clin Cancer Res. 2003;9(15):5714–20.
96. Beck R, et al. Pretreatment 18F-FAZA PET predicts success of hypoxia-directed radiochemotherapy using tirapazamine. J Nucl Med. 2007;48(6):973–80.
97. von Pawel J, et al. Tirapazamine plus cisplatin versus cisplatin in advanced non-small-cell lung cancer: a report of the international CATAPULT I study group. Cisplatin and tirapazamine in subjects with advanced previously untreated non-small-cell lung tumors. J Clin Oncol. 2000;18(6):1351–9.
98. Brizel DM, et al. Oxygenation of head and neck cancer: changes during radiotherapy and impact on treatment outcome. Radiother Oncol. 1999;53(2): 113–7.
99. Grosu AL, et al. Hypoxia imaging with FAZA-PET and theoretical considerations with regard to dose painting for individualization of radiotherapy in patients with head and neck cancer. Int J Radiat Oncol Biol Phys. 2007;69(2):541–51.
100. O'Tuama LA, et al. Two-phase [11C]L-methionine PET in childhood brain tumors. Pediatr Neurol. 1990;6(3):163–70.
101. Utriainen M, et al. Metabolic characterization of childhood brain tumors: comparison of 18F-fluorodeoxyglucose and 11C-methionine positron emission tomography. Cancer. 2002;95(6): 1376–86.
102. Virgolini I, et al. Procedure guidelines for PET/CT tumour imaging with 68Ga-DOTA-conjugated peptides: 68Ga-DOTA-TOC, 68Ga-DOTA-NOC, 68Ga-DOTA-TATE. Eur J Nucl Med Mol Imaging. 2010;37(10):2004–10.
103. Shulkin BL, et al. PET hydroxyephedrine imaging of neuroblastoma. J Nucl Med. 1996;37(1):16–21.
104. Sisson JC, Shulkin BL. Nuclear medicine imaging of pheochromocytoma and neuroblastoma. Q J Nucl Med. 1999;43(3):217–23.
105. Hoegerle S, et al. Pheochromocytomas: detection with 18F DOPA whole body PET--initial results. Radiology. 2002;222(2):507–12.
106. deKemp RA, Nahmias C. Attenuation correction in PET using single photon transmission measurement. Med Phys. 1994;21(6):771–8.
107. Biermann M, et al. Is there a role for PET-CT and SPECT-CT in pediatric oncology? Acta Radiol. 2013;54(9):1037–45.
108. Srinivasan M, Bhaskar S, Carlson DW. Variation in procedural sedation practices among Children's Hospitals. Hosp Pediatr. 2015;5(3):148–53.
109. Martinez-Moller A, Nekolla SG. Attenuation correction for PET/MR: problems, novel approaches and practical solutions. Z Med Phys. 2012;22(4):299–310.
110. Roy S, et al. PET attenuation correction using synthetic CT from ultrashort echo-time MR imaging. J Nucl Med. 2014;55(12):2071–7.
111. Berker Y, Kiessling F, Schulz V. Scattered PET data for attenuation-map reconstruction in PET/MRI. Med Phys. 2014;41(10):102502.
112. Yip S, et al. Sensitivity study of voxel-based PET image comparison to image registration algorithms. Med Phys. 2014;41(11):111714.
113. Kinney H, Faix R, Brazy J. The fetal alcohol syndrome and neuroblastoma. Pediatrics. 1980;66(1): 130–2.
114. Kramer S, et al. Medical and drug risk factors associated with neuroblastoma: a case–control study. J Natl Cancer Inst. 1987;78(5):797–804.
115. Michalek AM, et al. Gravid health status, medication use, and risk of neuroblastoma. Am J Epidemiol. 1996;143(10):996–1001.
116. Bunin GR, et al. Neuroblastoma and parental occupation. Am J Epidemiol. 1990;131(5):776–80.
117. Strenger V, et al. Diagnostic and prognostic impact of urinary catecholamines in neuroblastoma patients. Pediatr Blood Cancer. 2007;48(5):504–9.
118. Maris JM. Recent advances in neuroblastoma. N Engl J Med. 2010;362(23):2202–11.
119. Kushner BH. Neuroblastoma: a disease requiring a multitude of imaging studies. J Nucl Med. 2004;45(7):1172–88.
120. Olivier P, et al. Guidelines for radioiodinated MIBG scintigraphy in children. Eur J Nucl Med Mol Imaging. 2003;30(5):B45–50.
121. Lonergan GJ, et al. Neuroblastoma, ganglioneuroblastoma, and ganglioneuroma: radiologic-pathologic correlation. Radiographics. 2002;22(4):911–34.
122. Howman-Giles RB, Gilday DL, Ash JM. Radionuclide skeletal survey in neuroblastoma. Radiology. 1979;131(2):497–502.
123. Sharp SE, et al. 123I-MIBG scintigraphy and 18F-FDG PET in neuroblastoma. J Nucl Med. 2009;50(8):1237–43.
124. Choi YJ, et al. (18)F-FDG PET as a single imaging modality in pediatric neuroblastoma: comparison with abdomen CT and bone scintigraphy. Ann Nucl Med. 2014;28(4):304–13.
125. Taggart DR, et al. Comparison of iodine-123 metaiodobenzylguanidine (MIBG) scan and [18F] fluorodeoxyglucose positron emission tomography to evaluate response after iodine-131 MIBG therapy for relapsed neuroblastoma. J Clin Oncol. 2009;27(32):5343–9.
126. Piccardo A, et al. Comparison of 18F-dopa PET/CT and 123I-MIBG scintigraphy in stage 3 and 4 neuroblastoma: a pilot study. Eur J Nucl Med Mol Imaging. 2012;39(1):57–71.
127. Pashankar FD, O'Dorisio MS, Menda Y. MIBG and somatostatin receptor analogs in children: current concepts on diagnostic and therapeutic use. J Nucl Med. 2005;46 Suppl 1:55S–61.
128. Kroiss A, et al. Functional imaging in phaeochromocytoma and neuroblastoma with 68Ga-DOTA-Tyr3-octreotide positron emission tomography and 123I-metaiodobenzylguanidine: a clarification. Eur J Nucl Med Mol Imaging. 2012;39(3):543.

129. De Krijger RR, et al. Frequent genetic changes in childhood pheochromocytomas. Ann N Y Acad Sci. 2006;1073:166–76.
130. Pacak K, et al. Biochemical diagnosis, localization and management of pheochromocytoma: focus on multiple endocrine neoplasia type 2 in relation to other hereditary syndromes and sporadic forms of the tumour. J Intern Med. 2005;257(1):60–8.
131. Pacak K, Eisenhofer G, Grossman A. The incidentally discovered adrenal mass. N Engl J Med. 2007;356(19):2005.
132. Pacak K, et al. Pheochromocytoma: recommendations for clinical practice from the First International Symposium. October 2005. Nat Clin Pract Endocrinol Metab. 2007;3(2):92–102.
133. Havekes B, et al. Update on pediatric pheochromocytoma. Pediatr Nephrol. 2009;24(5):943–50.
134. Trampal C, et al. Pheochromocytomas: detection with 11C hydroxyephedrine PET. Radiology. 2004;230(2):423–8.
135. Janssen I, et al. Superiority of [68Ga]-DOTATATE PET/CT to other functional imaging modalities in the localization of SDHB-associated metastatic pheochromocytoma and paraganglioma. Clin Cancer Res. 2015;21:3888–95.
136. Brugieres L, Minard V, Patte C. Lymphomas in children and adolescents. Rev Prat. 2012;62(4):453–8.
137. Bhatia S, et al. High risk of subsequent neoplasms continues with extended follow-up of childhood Hodgkin's disease: report from the Late Effects Study Group. J Clin Oncol. 2003;21(23):4386–94.
138. Prasad PK, et al. Long-term non-cancer mortality in pediatric and young adult cancer survivors in Finland. Pediatr Blood Cancer. 2012;58(3):421–7.
139. Howman-Giles R, Stevens M, Bergin M. Role of gallium-67 in management of paediatric solid tumours. Aust Paediatr J. 1982;18(2):120–5.
140. Sty JR, Kun LE, Starshak RJ. Pediatric applications in nuclear oncology. Semin Nucl Med. 1985;15(2):171–200.
141. Elstrom R, et al. Utility of FDG-PET scanning in lymphoma by WHO classification. Blood. 2003;101(10):3875–6.
142. Rigacci L, et al. Positron emission tomography in the staging of patients with Hodgkin's lymphoma. A prospective multicentric study by the Intergruppo Italiano Linfomi. Ann Hematol. 2007;86(12):897–903.
143. Jerusalem G, et al. Whole-body positron emission tomography using 18F-fluorodeoxyglucose compared to standard procedures for staging patients with Hodgkin's disease. Haematologica. 2001;86(3):266–73.
144. London K, et al. 18F-FDG PET/CT in paediatric lymphoma: comparison with conventional imaging. Eur J Nucl Med Mol Imaging. 2011;38(2):274–84.
145. Hutchings M, et al. Position emission tomography with or without computed tomography in the primary staging of Hodgkin's lymphoma. Haematologica. 2006;91(4):482–9.
146. Kabickova E, et al. Comparison of 18F-FDG-PET and standard procedures for the pretreatment staging of children and adolescents with Hodgkin's disease. Eur J Nucl Med Mol Imaging. 2006;33(9):1025–31.
147. Moulin-Romsee G, et al. (18)F-FDG PET/CT bone/bone marrow findings in Hodgkin's lymphoma may circumvent the use of bone marrow trephine biopsy at diagnosis staging. Eur J Nucl Med Mol Imaging. 2010;37(6):1095–105.
148. Pelosi E, et al. FDG-PET in the detection of bone marrow disease in Hodgkin's disease and aggressive non-Hodgkin's lymphoma and its impact on clinical management. Q J Nucl Med Mol Imaging. 2008;52(1):9–16.
149. Purz S, et al. [18F]Fluorodeoxyglucose positron emission tomography for detection of bone marrow involvement in children and adolescents with Hodgkin's lymphoma. J Clin Oncol. 2011;29(26):3523–8.
150. Girinsky T, et al. Is FDG-PET scan in patients with early stage Hodgkin lymphoma of any value in the implementation of the involved-node radiotherapy concept and dose painting? Radiother Oncol. 2007;85(2):178–86.
151. Hermann S, et al. Staging in childhood lymphoma: differences between FDG-PET and CT. Nuklearmedizin. 2005;44(1):1–7.
152. Muslimani AA, et al. The utility of 18-F-fluorodeoxyglucose positron emission tomography in evaluation of bone marrow involvement by non-Hodgkin lymphoma. Am J Clin Oncol. 2008;31(5):409–12.
153. Kluge R, et al. FDG PET/CT in children and adolescents with lymphoma. Pediatr Radiol. 2013;43(4):406–17.
154. Weiler-Sagie M, et al. (18)F-FDG avidity in lymphoma readdressed: a study of 766 patients. J Nucl Med. 2010;51(1):25–30.
155. Abramson SJ, Price AP. Imaging of pediatric lymphomas. Radiol Clin North Am. 2008;46(2):313–38, ix.
156. Toma P, et al. Multimodality imaging of Hodgkin disease and non-Hodgkin lymphomas in children. Radiographics. 2007;27(5):1335–54.
157. Cheson BD, et al. Revised response criteria for malignant lymphoma. J Clin Oncol. 2007;25(5):579–86.
158. Cahu X, et al. 18F-fluorodeoxyglucose-positron emission tomography before, during and after treatment in mature T/NK lymphomas: a study from the GOELAMS group. Ann Oncol. 2011;22(3):705–11.
159. Karantanis D, et al. 18F-FDG PET and PET/CT in Burkitt's lymphoma. Eur J Radiol. 2010;75(1):e68–73.
160. Rini JN, et al. 18F-FDG PET versus CT for evaluating the spleen during initial staging of lymphoma. J Nucl Med. 2003;44(7):1072–4.

161. Seam P, Juweid ME, Cheson BD. The role of FDG-PET scans in patients with lymphoma. Blood. 2007;110(10):3507–16.
162. Rhodes MM, et al. Utility of FDG-PET/CT in follow-up of children treated for Hodgkin and non-Hodgkin lymphoma. J Pediatr Hematol Oncol. 2006;28(5):300–6.
163. Furth C, et al. Early and late therapy response assessment with [18F]fluorodeoxyglucose positron emission tomography in pediatric Hodgkin's lymphoma: analysis of a prospective multicenter trial. J Clin Oncol. 2009;27(26):4385–91.
164. Kostakoglu L, et al. PET predicts prognosis after 1 cycle of chemotherapy in aggressive lymphoma and Hodgkin's disease. J Nucl Med. 2002;43(8): 1018–27.
165. Kluge R, Korholz D. Role of FDG-PET in staging and therapy of children with Hodgkin lymphoma. Klin Padiatr. 2011;223(6):315–9.
166. Radford J, et al. Results of a trial of PET-directed therapy for early-stage Hodgkin's lymphoma. N Engl J Med. 2015;372(17):1598–607.
167. Duhrsen U, et al. Positron emission tomography guided therapy of aggressive non-Hodgkin lymphomas--the PETAL trial. Leuk Lymphoma. 2009;50(11):1757–60.
168. Depas G, et al. 18F-FDG PET in children with lymphomas. Eur J Nucl Med Mol Imaging. 2005;32(1): 31–8.
169. Bakhshi S, et al. Pediatric nonlymphoblastic non-Hodgkin lymphoma: baseline, interim, and post-treatment PET/CT versus contrast-enhanced CT for evaluation--a prospective study. Radiology. 2012;262(3):956–68.
170. Lavely WC, et al. FDG PET in the follow-up management of patients with newly diagnosed Hodgkin and non-Hodgkin lymphoma after first-line chemotherapy. Int J Radiat Oncol Biol Phys. 2003;57(2): 307–15.
171. Burns DM, Crawford DH. Epstein-Barr virus-specific cytotoxic T-lymphocytes for adoptive immunotherapy of post-transplant lymphoproliferative disease. Blood Rev. 2004;18(3):193–209.
172. Blaes AH, Morrison VA. Post-transplant lymphoproliferative disorders following solid-organ transplantation. Expert Rev Hematol. 2010;3(1):35–44.
173. Taylor AL, Marcus R, Bradley JA. Post-transplant lymphoproliferative disorders (PTLD) after solid organ transplantation. Crit Rev Oncol Hematol. 2005;56(1):155–67.
174. Feng S, et al. Tumors and transplantation: the 2003 Third Annual ASTS State-of-the-Art Winter Symposium. Am J Transplant. 2003;3(12):1481–7.
175. Dharnidharka VR, et al. Post-transplant lymphoproliferative disorder in the United States: young Caucasian males are at highest risk. Am J Transplant. 2002;2(10):993–8.
176. Shapiro R, et al. Posttransplant lymphoproliferative disorders in adult and pediatric renal transplant patients receiving tacrolimus-based immunosuppression. Transplantation. 1999;68(12):1851–4.
177. Leblond V, et al. Lymphoproliferative disorders after organ transplantation: a report of 24 cases observed in a single center. J Clin Oncol. 1995;13(4):961–8.
178. Opelz G, Dohler B. Lymphomas after solid organ transplantation: a collaborative transplant study report. Am J Transplant. 2004;4(2):222–30.
179. Gallego S, et al. Post-transplant lymphoproliferative disorders in children: the role of chemotherapy in the era of rituximab. Pediatr Transplant. 2010;14(1): 61–6.
180. Campo E, et al. The 2008 WHO classification of lymphoid neoplasms and beyond: evolving concepts and practical applications. Blood. 2011;117(19): 5019–32.
181. Bianchi E, et al. Clinical usefulness of FDG-PET/CT scan imaging in the management of posttransplant lymphoproliferative disease. Transplantation. 2008;85(5):707–12.
182. Dierickx D, et al. The accuracy of positron emission tomography in the detection of posttransplant lymphoproliferative disorder. Haematologica. 2013;98(5):771–5.
183. O'Conner AR, Franc BL. FDG PET imaging in the evaluation of post-transplant lymphoproliferative disorder following renal transplantation. Nucl Med Commun. 2005;26(12):1107–11.
184. Takehana CS, et al. (18)F-FDG PET/CT in the management of patients with post-transplant lymphoproliferative disorder. Nucl Med Commun. 2014;35(3):276–81.
185. Bakker NA, et al. PTLD visualization by FDG-PET: improved detection of extranodal localizations. Am J Transplant. 2006;6(8):1984–5.
186. Noraini AR, et al. PET-CT as an effective imaging modality in the staging and follow-up of post-transplant lymphoproliferative disorder following solid organ transplantation. Singapore Med J. 2009;50(12):1189–95.
187. Panagiotidis E, et al. (18)F-fluorodeoxyglucose positron emission tomography/computed tomography in diagnosis of post-transplant lymphoproliferative disorder. Leuk Lymphoma. 2014;55(3):515–9.
188. von Falck C, et al. Post transplant lymphoproliferative disease in pediatric solid organ transplant patients: a possible role for [18F]-FDG-PET(/CT) in initial staging and therapy monitoring. Eur J Radiol. 2007;63(3):427–35.
189. Su K, et al. Diffuse homogeneous bone marrow uptake of FDG in patients with acute lymphoblastic leukemia. Clin Nucl Med. 2013;38(1):e33–4.
190. Endo T, et al. Localized relapse in bone marrow of extremities after allogeneic stem cell transplantation for acute lymphoblastic leukemia. Am J Hematol. 2004;76(3):279–82.
191. Sharp SE, Gelfand MJ, Absalon MJ. Altered FDG uptake patterns in pediatric lymphoblastic lymphoma patients receiving induction chemotherapy

that includes very high dose corticosteroids. Pediatr Radiol. 2012;42(3):331–6.
192. Stanescu L, et al. FDG PET of the brain in pediatric patients: imaging spectrum with MR imaging correlation. Radiographics. 2013;33(5):1279–303.
193. Kruer MC, et al. The value of positron emission tomography and proliferation index in predicting progression in low-grade astrocytomas of childhood. J Neurooncol. 2009;95(2):239–45.
194. Borgwardt L, et al. Increased fluorine-18 2-fluoro-2-deoxy-D-glucose (FDG) uptake in childhood CNS tumors is correlated with malignancy grade: a study with FDG positron emission tomography/magnetic resonance imaging coregistration and image fusion. J Clin Oncol. 2005;23(13):3030–7.
195. Glantz MJ, et al. Identification of early recurrence of primary central nervous system tumors by [18F]fluorodeoxyglucose positron emission tomography. Ann Neurol. 1991;29(4):347–55.
196. Hanson MW, et al. FDG-PET in the selection of brain lesions for biopsy. J Comput Assist Tomogr. 1991;15(5):796–801.
197. Giovannini E, et al. Clinical applications of choline PET/CT in brain tumors. Curr Pharm Des. 2015;21(1):121–7.
198. Torii K, et al. Correlation of amino-acid uptake using methionine PET and histological classifications in various gliomas. Ann Nucl Med. 2005;19(8):677–83.
199. Ceyssens S, et al. [11C]methionine PET, histopathology, and survival in primary brain tumors and recurrence. AJNR Am J Neuroradiol. 2006;27(7):1432–7.
200. Van Laere K, et al. Direct comparison of 18F-FDG and 11C-methionine PET in suspected recurrence of glioma: sensitivity, inter-observer variability and prognostic value. Eur J Nucl Med Mol Imaging. 2005;32(1):39–51.
201. Hipp SJ, et al. Molecular imaging of pediatric brain tumors: comparison of tumor metabolism using (1)(8)F-FDG-PET and MRSI. J Neurooncol. 2012;109(3):521–7.
202. Gilday DL, Ash JM, Reilly BJ. Radionuclide skeletal survey for pediatric neoplasms. Radiology. 1977;123(2):399–406.
203. Rosen G, et al. Serial thallium-201 scintigraphy in osteosarcoma. Correlation with tumor necrosis after preoperative chemotherapy. Clin Orthop Relat Res. 1993;293:302–6.
204. Ramanna L, et al. Thallium-201 scintigraphy in bone sarcoma: comparison with gallium-67 and technetium-MDP in the evaluation of chemotherapeutic response. J Nucl Med. 1990;31(5):567–72.
205. Volker T, et al. Positron emission tomography for staging of pediatric sarcoma patients: results of a prospective multicenter trial. J Clin Oncol. 2007;25(34):5435–41.
206. Byun BH, et al. Comparison of (18)F-FDG PET/CT and (99 m)Tc-MDP bone scintigraphy for detection of bone metastasis in osteosarcoma. Skeletal Radiol. 2013;42(12):1673–81.
207. Huang TL, et al. Comparison between F-18-FDG positron emission tomography and histology for the assessment of tumor necrosis rates in primary osteosarcoma. J Chin Med Assoc. 2006;69(8):372–6.
208. Mansky PJ, et al. Treatment of metastatic osteosarcoma with the somatostatin analog OncoLar: significant reduction of insulin-like growth factor-1 serum levels. J Pediatr Hematol Oncol. 2002;24(6):440–6.
209. Kong CB, et al. (1)(8)F-FDG PET SUVmax as an indicator of histopathologic response after neoadjuvant chemotherapy in extremity osteosarcoma. Eur J Nucl Med Mol Imaging. 2013;40(5):728–36.
210. Erlemann R, et al. Response of osteosarcoma and Ewing sarcoma to preoperative chemotherapy: assessment with dynamic and static MR imaging and skeletal scintigraphy. Radiology. 1990;175(3):791–6.
211. Gaston LL, et al. 18F-FDG PET response to neoadjuvant chemotherapy for Ewing sarcoma and osteosarcoma are different. Skeletal Radiol. 2011;40(8):1007–15.
212. Tateishi U, et al. Comparative study of FDG PET/CT and conventional imaging in the staging of rhabdomyosarcoma. Ann Nucl Med. 2009;23(2):155–61.
213. Klem ML, et al. PET for staging in rhabdomyosarcoma: an evaluation of PET as an adjunct to current staging tools. J Pediatr Hematol Oncol. 2007;29(1):9–14.
214. Adler LP, et al. Noninvasive grading of musculoskeletal tumors using PET. J Nucl Med. 1991;32(8):1508–12.
215. Ricard F, et al. Additional benefit of F-18 FDG PET/CT in the staging and follow-up of pediatric rhabdomyosarcoma. Clin Nucl Med. 2011;36(8):672–7.
216. Moinul Hossain AK, et al. FDG positron emission tomography/computed tomography studies of Wilms' tumor. Eur J Nucl Med Mol Imaging. 2010;37(7):1300–8.
217. Qin Z, et al. Use of 18F-FDG-PET-CT for assessment of response to neoadjuvant chemotherapy in children with Wilms tumor. J Pediatr Hematol Oncol. 2015;37:396–401.
218. Wong KK, et al. The use of positron emission tomography in detecting hepatoblastoma recurrence--a cautionary tale. J Pediatr Surg. 2004;39(12):1779–81.
219. Mody RJ, et al. FDG PET for the study of primary hepatic malignancies in children. Pediatr Blood Cancer. 2006;47(1):51–5.
220. Ciarallo A, et al. Value of fluorodeoxyglucose PET/computed tomography patient management and outcomes in thyroid cancer. PET Clin. 2015;10(2):265–78.
221. Asa S, et al. The role of FDG-PET/CT in differentiated thyroid cancer patients with negative iodine-131 whole-body scan and elevated anti-Tg level. Ann Nucl Med. 2014;28(10):970–9.

222. Elboga U, et al. F-18 FDG PET/CT imaging in the diagnostic work-up of thyroid cancer patients with high serum thyroglobulin, negative I-131 whole body scan and suppressed thyrotropin: 8-year experience. Eur Rev Med Pharmacol Sci. 2015;19(3):396–401.
223. Beheshti M, et al. The value of 18F-DOPA PET-CT in patients with medullary thyroid carcinoma: comparison with 18F-FDG PET-CT. Eur Radiol. 2009;19(6):1425–34.
224. Howe TC, et al. Role of Tc-99m DMSA (V) scanning and serum calcitonin monitoring in the management of medullary thyroid carcinoma. Singapore Med J. 2008;49(1):19–22.